

# **Becker & Hickl GmbH**

**DCS-120**

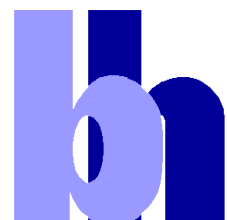
**Confocal and Multiphoton  
FLIM Systems**

with

**SPCImage NG FLIM Data Analysis**

**An Overview**

**2021**





## DCS-120 FLIM System

Becker & Hickl GmbH

Nunsdorfer Ring 7-9

12277 Berlin

Germany

Tel. +49 / 30 / 212 800 20

FAX +49 / 30 / 212 800 213

<http://www.becker-hickl.com>

email: [info@becker-hickl.com](mailto:info@becker-hickl.com)

October 2021

This brochure is subject to copyright. However, reproduction of small portions of the material in scientific papers or other non-commercial publications is considered fair use under the copyright law. It is requested that a complete citation be included in the publication. If you require confirmation please feel free to contact Becker & Hickl.

# DCS-120 Confocal and Multiphoton FLIM Systems

*Abstract:* The DCS-120 system uses excitation by ps diode lasers or femtosecond titanium-sapphire lasers, fast scanning by galvanometer mirrors, confocal detection, and FLIM by bh's multidimensional TCSPC technique to record fluorescence lifetime images at high temporal resolution, high spatial resolution, and high sensitivity [3]. The DCS-120 system is available with inverted microscopes of Nikon, Zeiss, and Olympus. It can also be used to convert an existing conventional microscope into a fully functional confocal or multiphoton laser scanning microscope with TCSPC detection. Due to its fast beam scanning and its high sensitivity the DCS-120 system is compatible with live-cell imaging. DCS-120 functions include simultaneous recording of FLIM or steady-state fluorescence images simultaneously in two fully parallel wavelength channels, laser wavelength multiplexing, time-series FLIM, time-series recording, Z stack FLIM, phosphorescence lifetime imaging (PLIM), fluorescence lifetime-transient scanning (FLITS) and FCS recording. Applications focus on lifetime variations by interactions of fluorophores with their molecular environment. Typical applications are ion concentration measurement, FRET experiments, metabolic imaging, and plant physiology.

## Introduction

The DCS-120 systems are complete laser scanning microscopes for fluorescence lifetime imaging. The systems use bh's multi-dimensional TCSPC FLIM technology [25, 31, 33] in combination with fast laser scanning and confocal detection or multi-photon excitation [34]. DCS-120 systems are available with various inverted and upright microscopes, see Fig. 1 and Fig. 2. A 'DCS-120 MACRO' system is available for FLIM of centimetre-size objects, see Fig. 2, second row, right. Advanced versions of the DCS-120 system are available for multiphoton excitation with Ti:Sa lasers and femtosecond fibre lasers (Fig. 2, bottom). The system also works with tuneable excitation sources [7, 9, 10]. Moreover, the DCS-120 scan head with the associated control and data acquisition electronics can be used to upgrade a conventional microscope with scanning and FLIM recording.

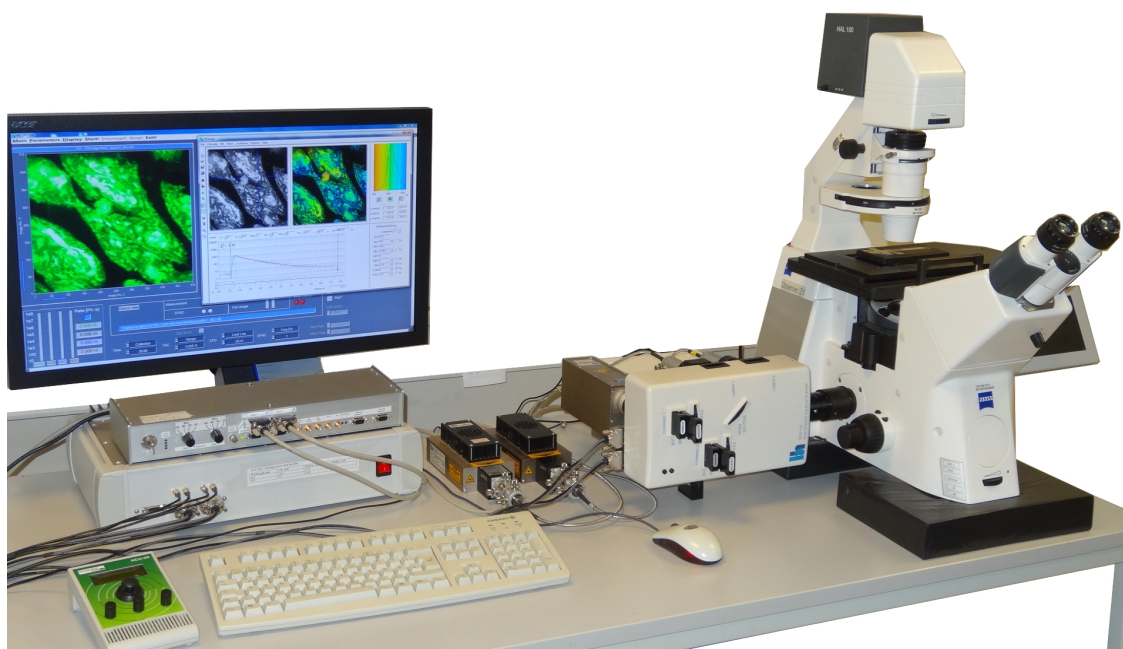


Fig. 1: The DCS-120 system with a Zeiss Axio Observer microscope

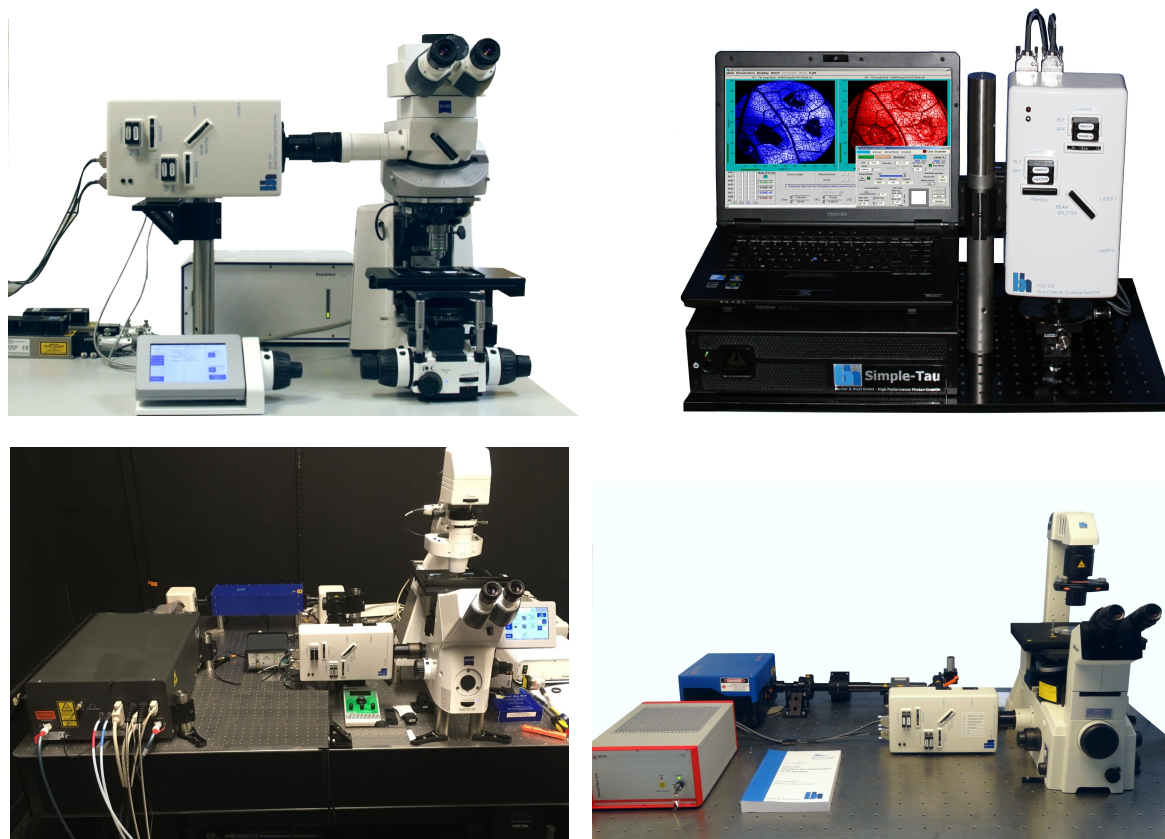


Fig. 2: Upper row: DCS-120 Axio Observer system, DCS-120 MACRO system. Lower row: DCS-120 MP multiphoton system with Ti:Sa laser, DCS-120 MP multiphoton with femtosecond fibre laser

In the basic configuration, the DCS-120 uses excitation by two ps diode lasers and records in two fully parallel detector and TCSPC channels. The systems are using highly efficient GaAsP hybrid detectors. By combining extremely high efficiency with large active area, high counting speed, high time-resolution, and low background, these detectors have initiated a breakthrough in FLIM recording [31]. Another step was made by the introduction of 64-bit data acquisition software [11, 79]. FLIM data are now recorded at unprecedented pixel numbers, high dynamic range, short acquisition time, and minimum exposure of the sample. New hardware and software functions have resulted in advanced FLIM functions, like time-series FLIM, Z stack FLIM, temporal Mosaic FLIM, wavelength-multiplexed FLIM, combined fluorescence and phosphorescence lifetime imaging (FLIM/PLIM), and fluorescence lifetime-transient scanning (FLITS). Due to its high sensitivity, the system can also be used for FCS recording and single-molecule spectroscopy. 16-channel multi-wavelength FLIM is available as an option. It uses a new multi-wavelength detector with a GaAsP cathode. Due to the high efficiency of the detector and the large memory space available in the 64 bit environment multi-wavelength FLIM can be recorded with unprecedented pixel numbers [11, 79]. Advanced versions of the DCS-120 system are available for multiphoton excitation and tuneable excitation sources [6, 7].

## Principle of Data Acquisition

### *Multi-Dimensional TCSPC*

The bh FLIM systems use a combination of bh's multidimensional time-correlated single-photon counting process with confocal or multiphoton laser scanning. The sample is continuously scanned by a high-repetition rate pulsed laser beam, single photons of the fluorescence signal are detected, and each photon is characterised by its time in the laser pulse period and the coordinates of the laser spot in

the scanning area in the moment of its detection. The recording process builds up a photon distribution over these parameters, see Fig. 3. The photon distribution can be interpreted as an array of pixels, each containing a full fluorescence decay curve in a large number of time channels.

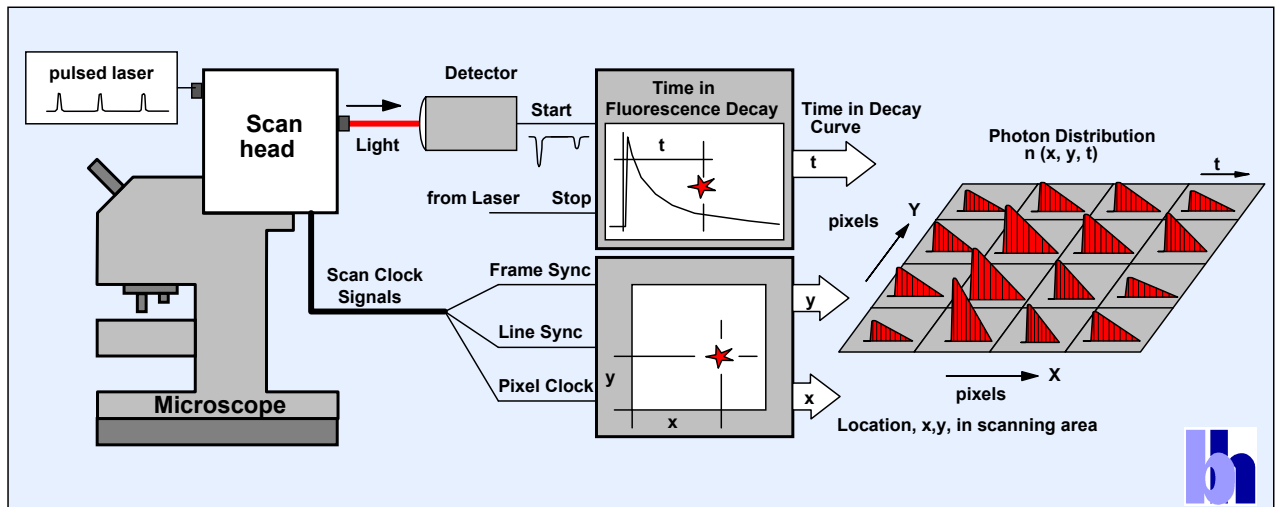


Fig. 3: Principle of TCSPC FLIM

The recording process delivers a near-ideal photon efficiency, excellent time resolution, and is independent of the speed of the scanner. The signal-to-noise ratio depends only on the total acquisition time and the photon rate available from the sample.

The technique can be extended by including additional parameters in the photon distribution. These can be the depth of the focus in the sample, the wavelength of the photons, the time after a stimulation of the sample, or the time within the period of an additional modulation of the laser. These techniques are used to record Z stacks or mosaics of FLIM images, multi-wavelength FLIM images, images of physiological effects occurring in the sample, or to record simultaneously fluorescence and phosphorescence lifetime images.

## Optical Principle

### Scanning

The principle of the scanner is shown in Fig. 4. Two laser beams are coupled into the scanner. They are combined by a beam combiner, pass the main beamsplitter, and are deflected by the scan mirrors. The scan lens sends the beam down the microscope beam path in a way that the scan mirror axis is projected into the back aperture of the microscope lens. The motion of the scan mirrors causes a variable tilt of the beam in the plane of the microscope lens. The laser is thus scanning an image area in the focal plane of the microscope lens. The scanning can be very fast - the line time can be as short as a millisecond, an entire frame can be scanned in less than a second.

### Confocal Scanning

The fluorescence light is collected back through the microscope lens, passes the scan lens, and is again reflected at the scan mirrors. The reflected beam is stationary, independently of the motion of the scan mirrors. It is separated into two spectral or polarisation components, and projected into confocal pinholes. The light signals passing the pinholes are filtered spectrally, and sent to the detectors. Only light from the excited spot in the focal plane of the microscope lens reaches the detectors. The result is a clear image from a defined depth inside the sample, without out-of-focus blur and lateral scattering.

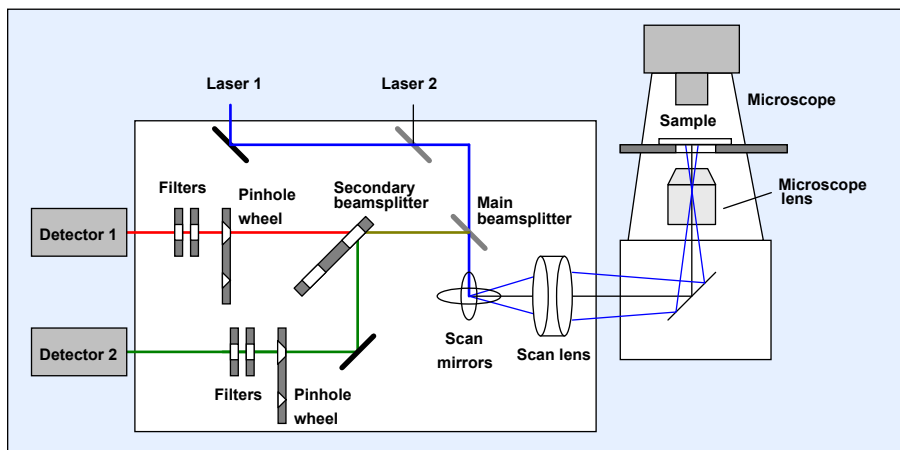


Fig. 4: Optical diagram of the DCS-120 scan head. Simplified, see [3] for details

The DCS-120 system is highly modular. The DCS-120 scan head is compatible with conventional microscopes of almost any type and manufacturer. Complete laser scanning systems are available with microscopes of Zeiss, Nikon, and Olympus. The DCS-120 MACRO system scans macroscopic objects directly in the image plane of the scan head. The DCS system can be used with a variety of different lasers and detectors. It can be operated with ps diode lasers of various wavelength, with tuneable excitation sources, and with fs lasers for multiphoton excitation.

### ***Multiphoton Excitation***

The DCS-120 MP version uses two-photon excitation by a titanium-sapphire laser. Due to the nonlinear nature of the two-photon process, excitation occurs only in a confined layer around the focal plane of the microscope lens. Two photon excitation has several advantages over one-photon excitation: First, the laser wavelength is in the NIR, where absorption and scattering coefficients are low. Consequently, deep layers of the sample can be reached. Second, fluorophores with excitation wavelengths in the UV can be reached without the need of UV optics. Third, since excitation occurs only in the focal plane, photochemical effects in the sample are reduced. A fourth advantage is that light scattered on the way out of the sample can efficiently be recorded without impairing the image quality.

### ***Non-Descanned detection***

Two-photon excitation occurs only in a thin layer around the focal plane of the microscope. Therefore, no pinhole is needed to suppress the detection of out-of focus fluorescence. Consequently, there is no need to send the fluorescence light all the way back through the scanner. Instead, the fluorescence is split from the excitation directly behind the microscope lens, and directly send to the detectors. The result is that even photons scattered on the way out of the sample have a chance to reach the detectors. The fact that scattered photons are detected does not impair the image quality - the data acquisition system automatically assigns them to the x-y position of the laser beam, not to the position where they left the sample. The result is high image quality and high detection efficiency from deep sample layers. The principle is shown in Fig. 5.

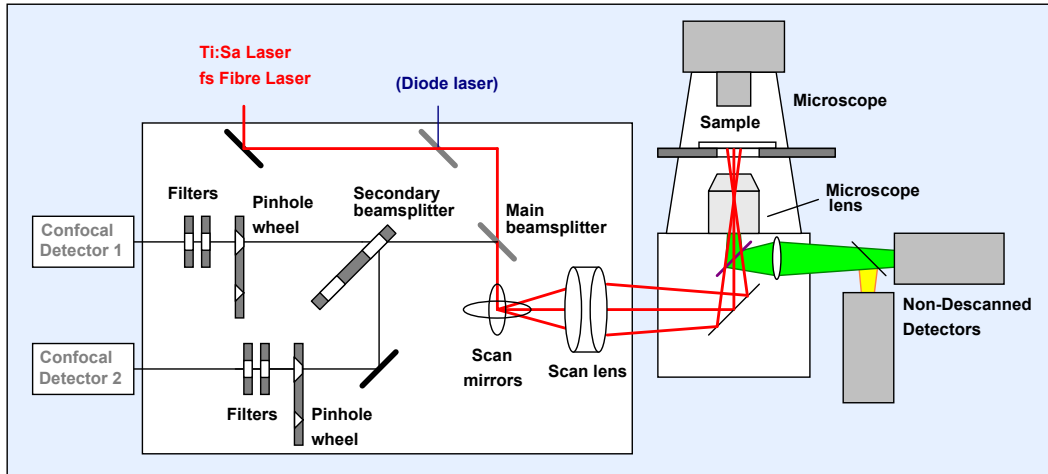


Fig. 5: Scanning with 2-photon excitation. Non-descanned detectors shown on the right.

On-photon excitation, two-photon excitation and descanned and non-descanned detectors can be combined in one system. In that case, a ps diode laser is injected via the second laser port, and the one-photon images are detected by confocal detectors. By enabling either the non-descanned detectors or the confocal detectors the system can be switched from one-photon and multiphoton operation and vice versa.

## DCS-120 Functions in Brief

### 64-bit SPCM Data Acquisition Software

The DCS-120 FLIM systems use the bh SPCM data acquisition software. Since 2013 the SPCM software is available in a 64-bit version. SPCM 64 bit exploits the full capability of Windows 64 bit, resulting in faster data processing, capability of recording images of extremely large pixel numbers, and availability of additional multi-dimensional FLIM modes [11, 31, 79]. The main panel of the SPCM data acquisition software is configurable by the user [31]. Different configurations for FLIM systems are shown in Fig. 6.

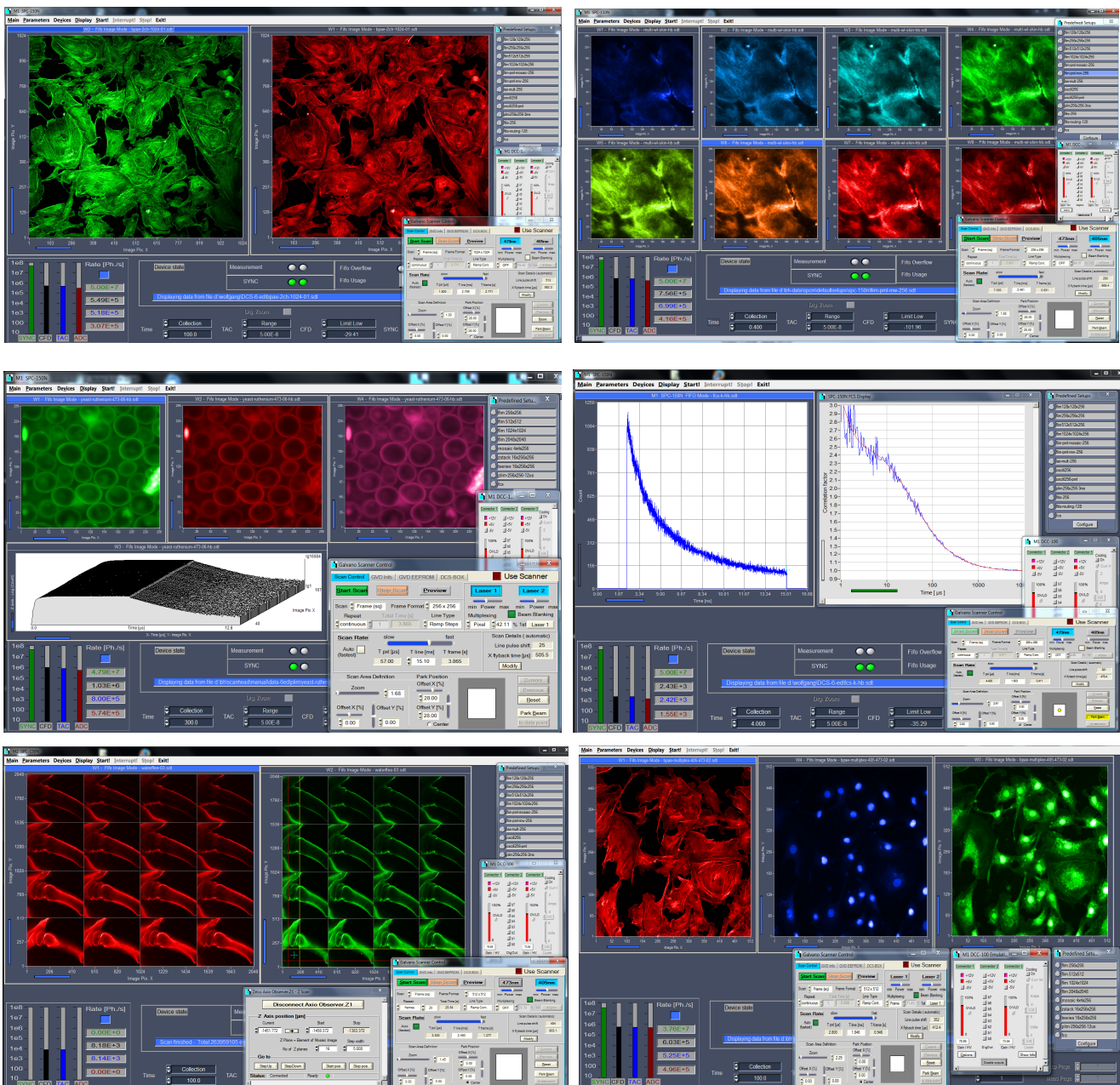


Fig. 6: SPCM software panel. Top left to bottom right: FLIM with two detector channels, multi-spectral FLIM, combined fluorescence / phosphorescence lifetime imaging (FLIM/PLIM), fluorescence correlation (FCS), Z-Stack FLIM, Excitation-wavelength multiplexed FLIM

### *Megapixel FLIM Images in Two Parallel Channels*

With 64 bit SPCM software pixel numbers can be increased to 2048 x 2048 pixels, with a temporal resolution of 256 time channels. Images are shown in Fig. 7 and Fig. 8 (facing page).

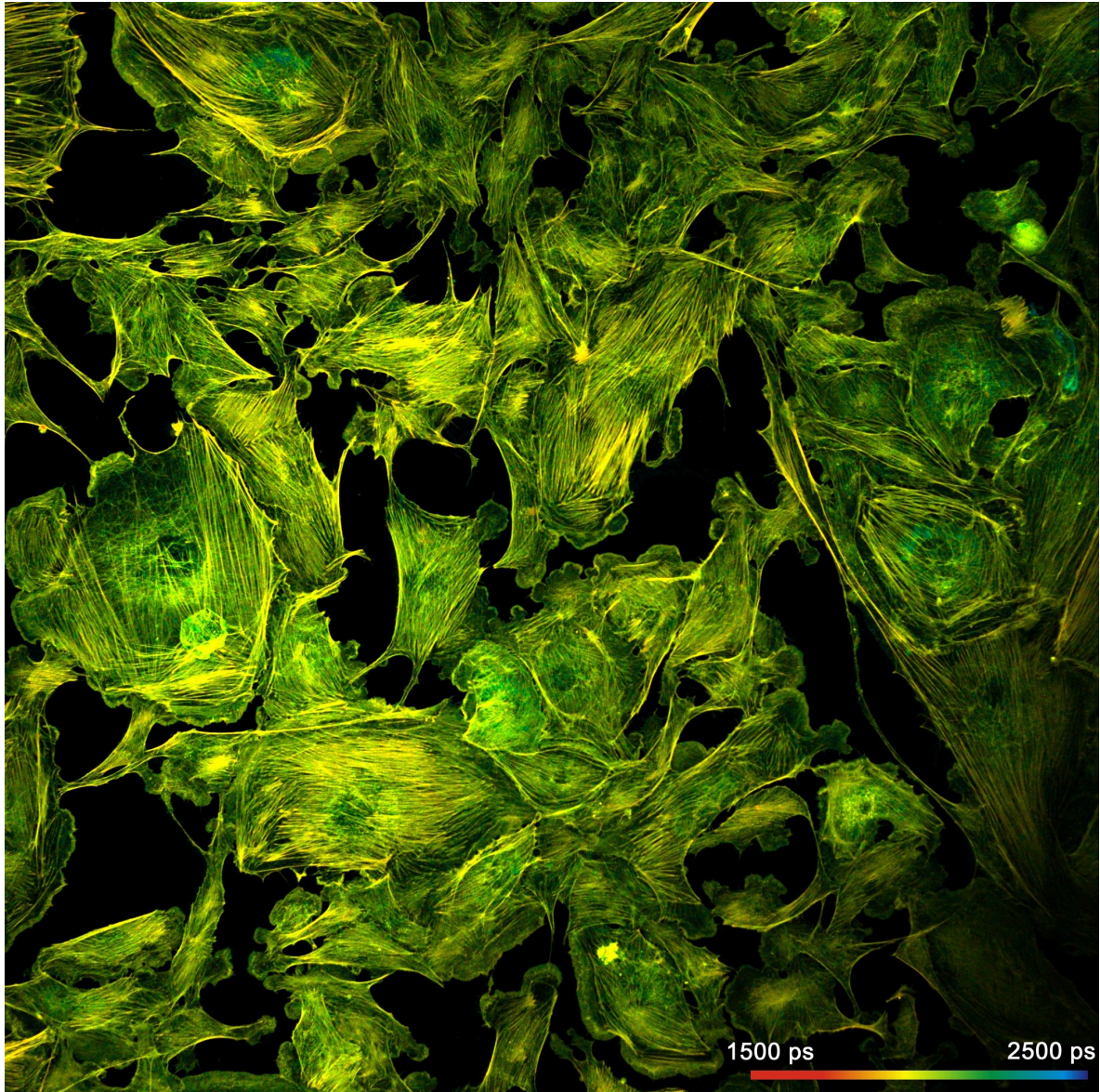


Fig. 7: BPAAE sample (Invitrogen) scanned with 2048 x 2048 pixels. Green channel, 485 to 560 nm

The DCS-120 system is able to simultaneously record two high-resolution images in different wavelength or polarisation channels, see Fig. 7 and Fig. 8. Recording is performed in two fully parallel TCSPC channels, avoiding any electronic lifetime or intensity crosstalk. Even if one channel should saturate the other is still producing correct data.

The capability to record images of large pixel numbers is beneficial for a wide range of FLIM applications. One example is tissue imaging where the samples are large, and the images are containing a wealth of detail. It is also useful when a large number of cells have to be investigated and the FLIM results to be compared. Megapixel FLIM records images of many cells simultaneously, and under exactly identical environment conditions. Moreover, the data are analysed in a single analysis

run, with identical IRFs and fit parameters. The results are therefore exactly comparable for all cells in the image area.

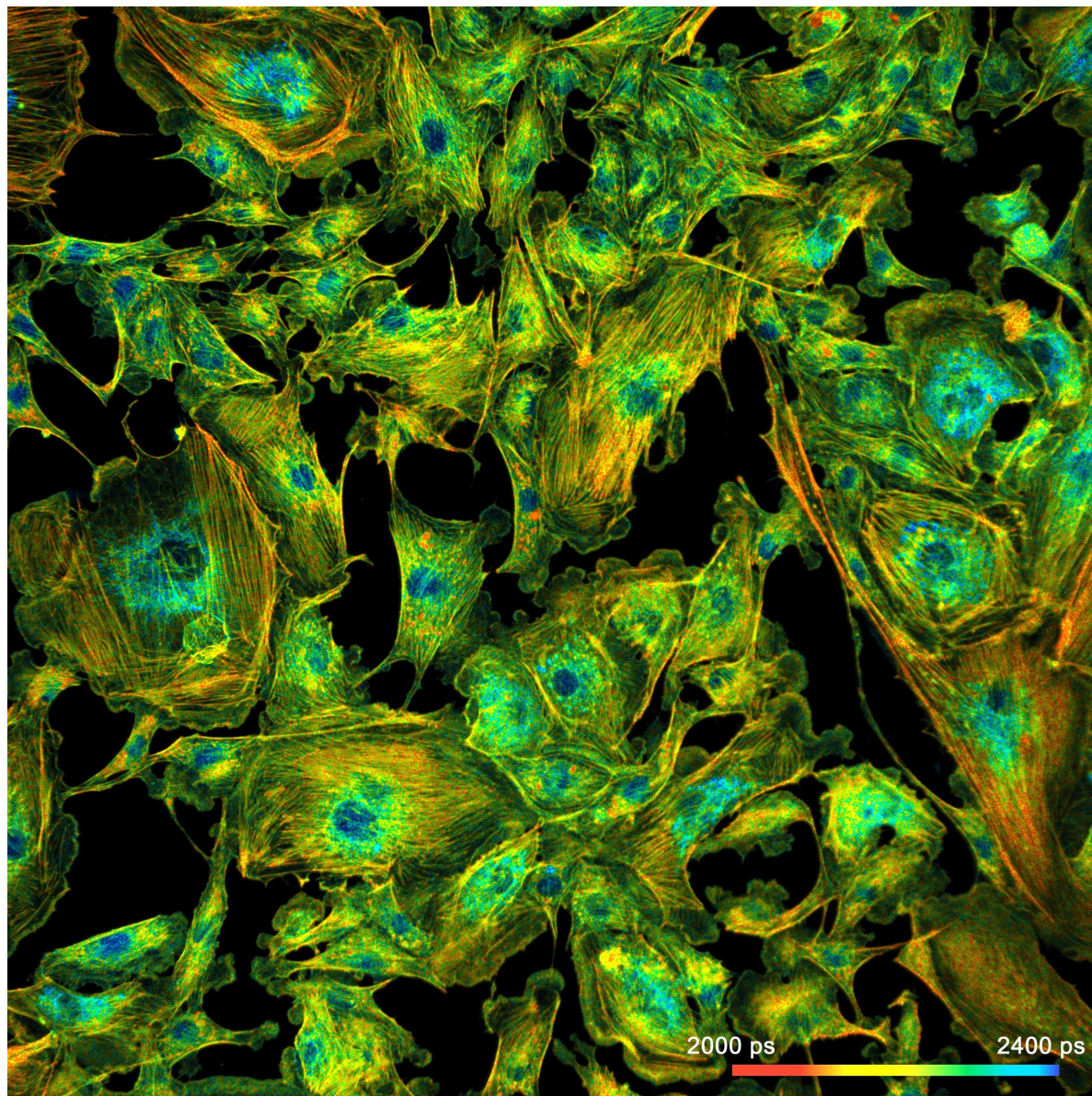


Fig. 8: BPAE sample (Invitrogen), scanned with 2048 x 2048 pixels. Red channel, 560 to 650 nm

### *Mosaic FLIM*

Mosaic FLIM records a large number of consecutive images into a single FLIM data array. The individual images within this array can represent the elements of a tile scan (x-y mosaic), images in different depth in the sample (z-stack mosaic), or images for different times after a stimulation of the sample (temporal mosaic). An example of an x-y mosaic is shown in Fig. 9. The complete data array has 2048 x 2048 pixels, and 256 time channels per pixel. Compared to a similar image taken through a low-magnification lens the advantage of mosaic FLIM is that a lens of high numerical aperture can be used, resulting in high detection efficiency and high spatial resolution.

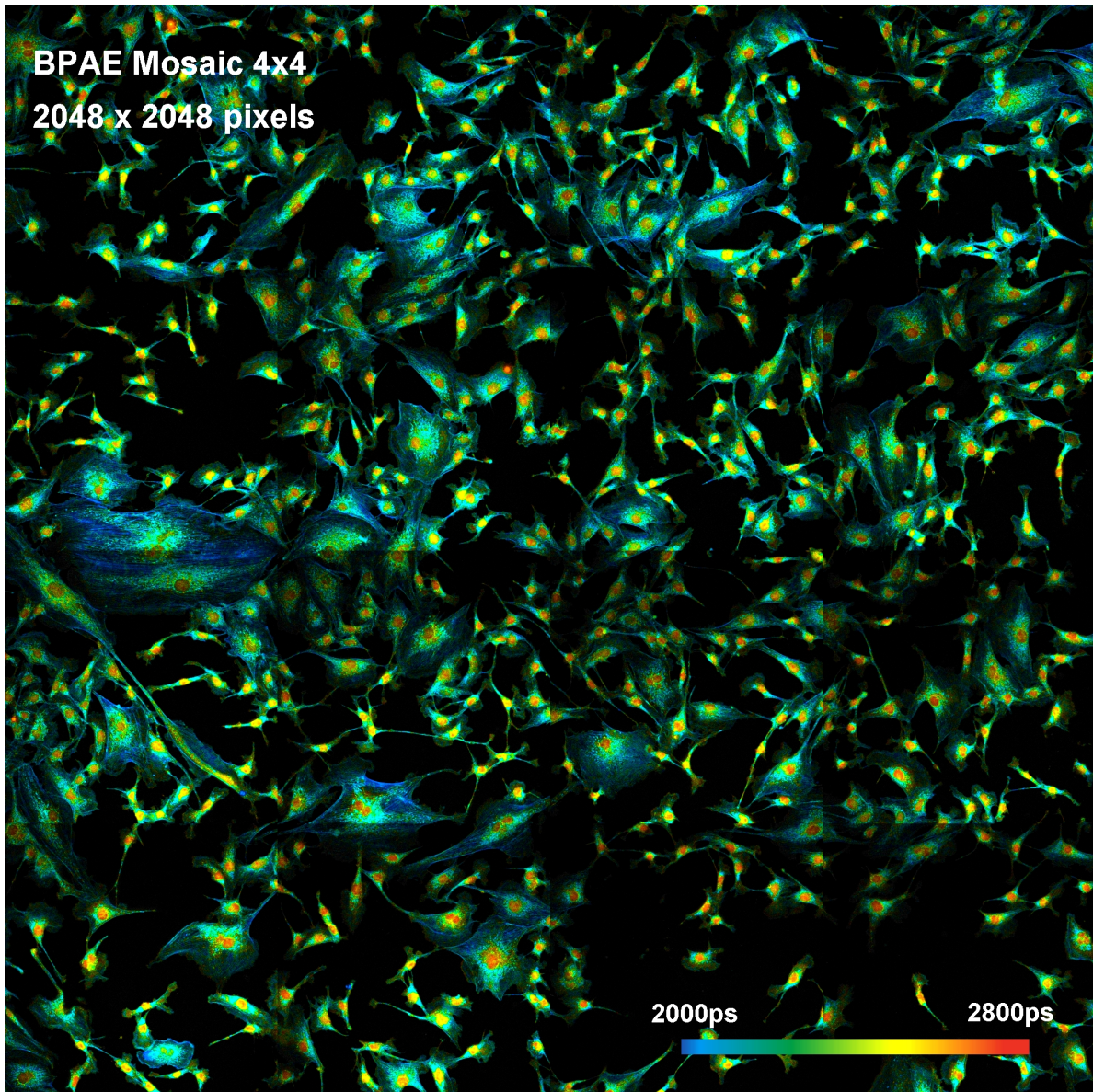


Fig. 9: Mosaic FLIM of a *Convallaria* sample. The mosaic has 4x4 elements, each element has 512x512 pixels with 256 time channels. The entire mosaic has 2048 x 2048 pixels, each pixel holding 256 time channels. DCS-120 MP multiphoton system with motorised sample stage.

### *Interactive Scanner Control*

The scanner control is fully integrated in the SPCM data acquisition software. The zoom factor and the position of the scan area can be adjusted via the scanner control panel or via the cursors of the display window. Changes in the scan parameters are executed online, without stopping the scan. Whatever you change in the microscope: The position of the samples, the scan area, the zoom factor, the focal plane, pinhole size or the laser power - the result becomes immediately visible in the preview images.

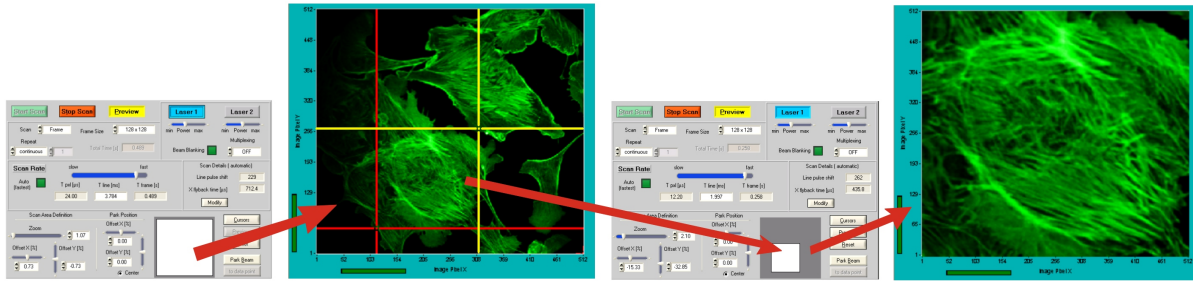


Fig. 10: Interactive scanner control

## Automatic Scanner Speed

Depending on the frame format and the zoom factor, the DCS-120 scanner control automatically selects the maximum speed of the scanner. The scanner thus always runs at high pixel rate, resulting in fast acquisition, minimum triplet excitation, and minimum photobleaching.

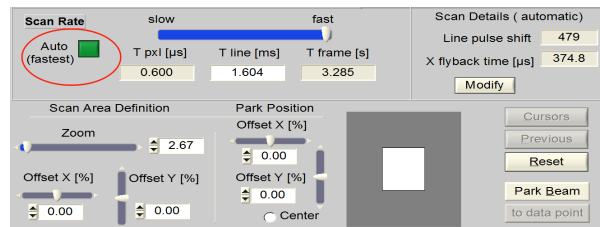


Fig. 11: Automatic selection of scan speed

## Easy Change Between Instrument Configurations

Frequently used instrument configurations are stored in a 'Predefined Setup' panel. Changing between the different configurations and user interfaces is just a matter of a single mouse click, see Fig. 12.

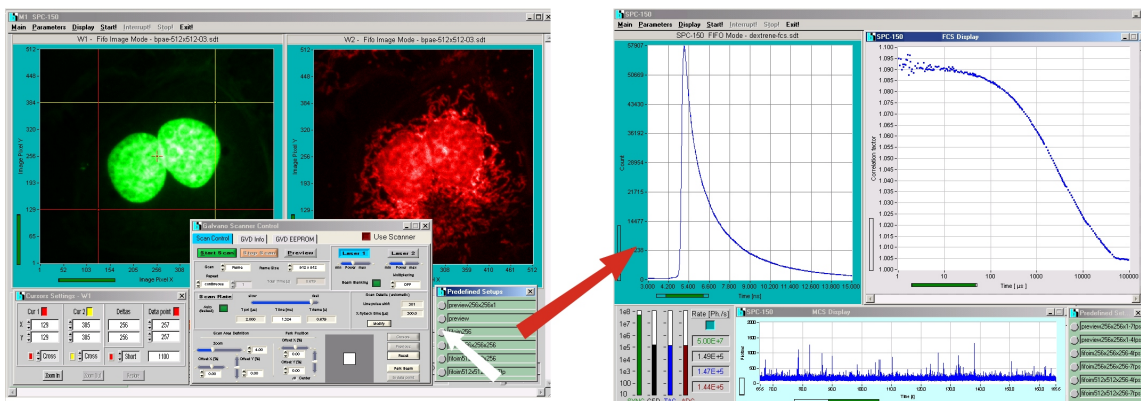


Fig. 12: Changing between different instrument configurations: The DCS-120 system switches from a FLIM configuration into an FCS configuration by a simple mouse click

## Fast Preview Function

When FLIM is applied to live samples the time and excitation dose needed for sample positioning, focusing, laser power adjustment, and region-of-interest selection has to be minimised. Therefore, the FLIM systems have a fast preview function. The preview function displays images in intervals on the order of 1 second and less, see Fig. 13.

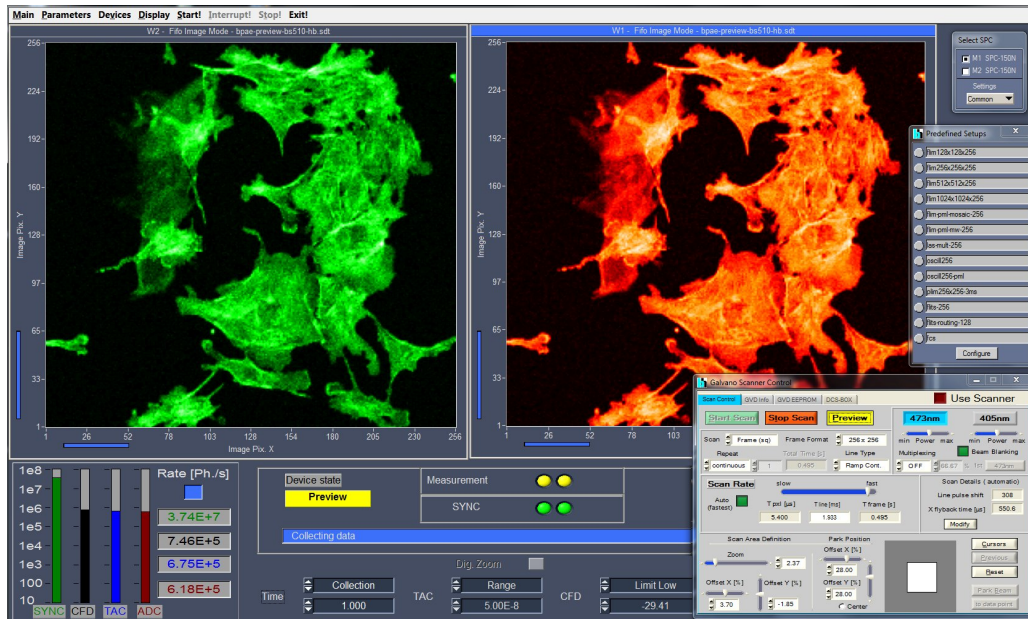


Fig. 13: SPCM software in fast preview mode, display rate one image per second.

### Online Lifetime Display

Starting from Version 9.72 SPCM software the DCS-120 system is able to display lifetime images online, both during the accumulation of FLIM data and for the individual steps of a fast image sequence [14]. Lifetime images can be displayed at images rates as fast as 10 images per second. The calculation of the lifetime images is based on the first moment of the decay data in the pixels of the images. The first-moment technique combines short calculation times with near-ideal photon efficiency. Importantly, it does not require to reduce the time resolution (time channels per pixel) to obtain high calculation speed. Even if the fast online lifetime function is used during the FLIM acquisition the data can later be processed by precision SPCImage multi-exponential data analysis.

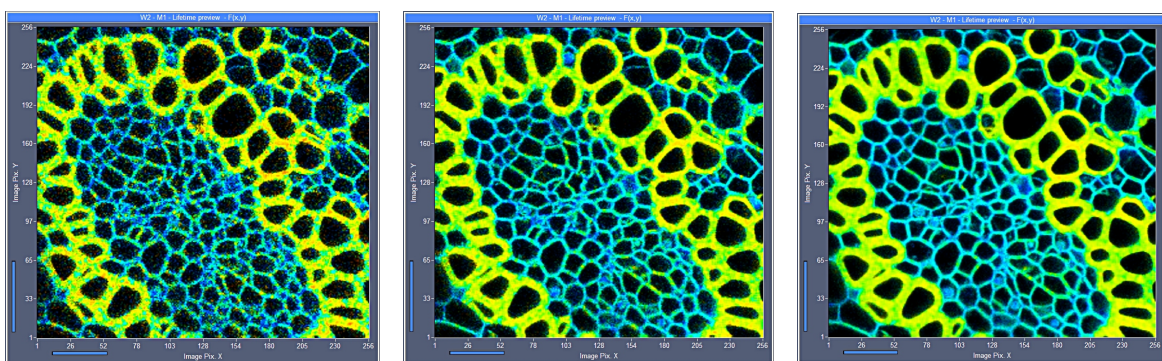


Fig. 14: 256x256-pixel images obtained by the online FLLIM display function. Acquisition time 0.2s, 0.5s, and 2s.

### Fast Beam Scanning - Fast Acquisition

The DCS-120 uses fast beam scanning by galvanometer mirrors. A complete frame is scanned within a time from 100 ms to a few seconds, with pixel dwell times down to one microsecond.

Compared with sample scanning, beam scanning is not only much faster, it avoids also induction of cell motion by exerting dynamic forces on the sample. Moreover, live cell imaging requires a fast preview function for sample positioning and focusing. This can only be provided if the beam is

scanned at a high frame rate. With its fast scanner and its multi-dimensional TCSPC process the DCS system achieves surprisingly short acquisition times, see Fig. 15.

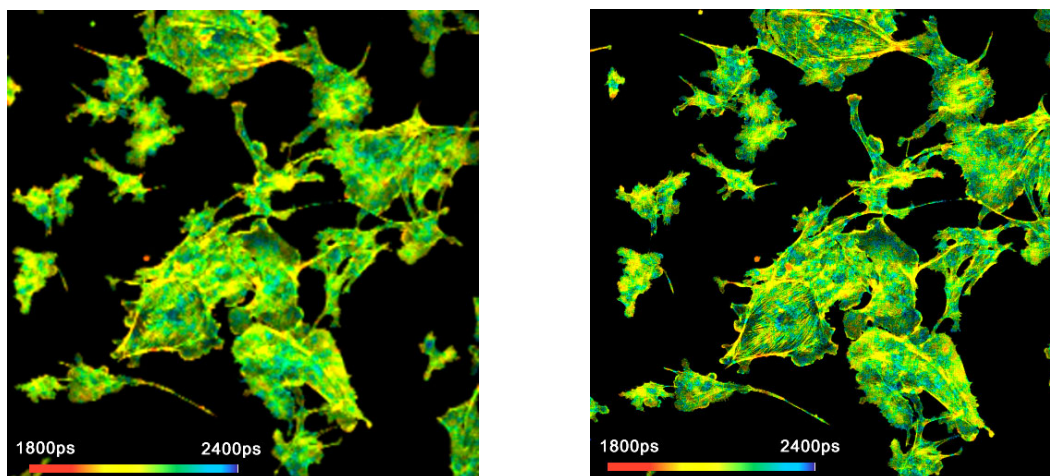


Fig. 15: FLIM images recorded within 5 seconds acquisition time. 256 x 256 pixels (left) and 512 x 512 pixels (right), both with 256 time channels.

Fast scanning is also the basis of recording fast FLIM time series. With the DCS-120 time-series can be recorded as fast as two images per second [58]. An example is shown in Fig. 16.

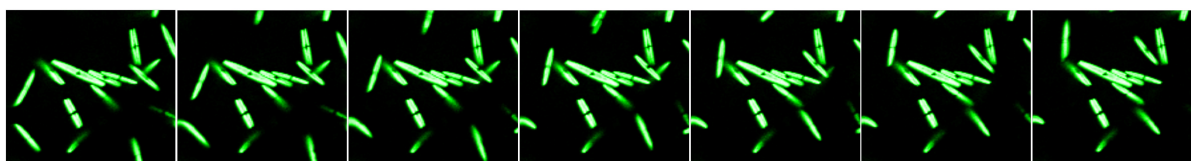


Fig. 16: Bacteria in motion. Autofluorescence, acquisition speed 2 images per second, scan speed 6 frames per second

### *Fast FLIM*

The DCS-120 system can be combined with the bh FASTAC Fast-Acquisition FLIM system. The FASTAC system uses four parallel TCSPC channels and a device that distributes the photon pulses of a single detector into the four recording channels. For details please see [17, 18] and [31].

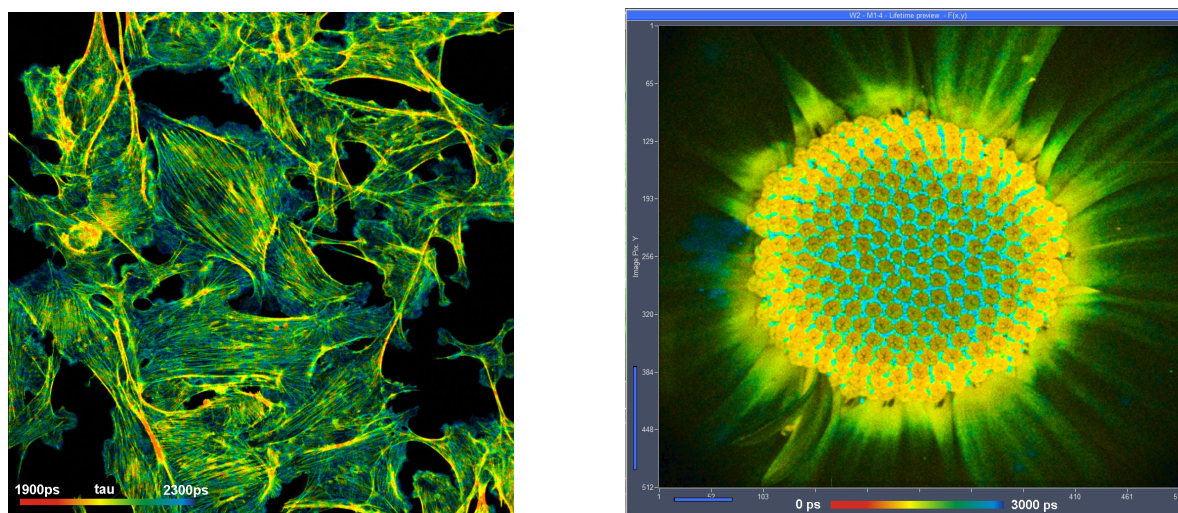


Fig. 17: Left: FASTAC 1024x1024-pixel image recorded with a DCS-120 system. Acquisition time 10 seconds. Right: 512x512-pixel image recorded with a DCS-120 MACRO system. Acquisition time 2 seconds.

## High-Efficiency High-Speed Hybrid Detectors

### *Ultra-High Efficiency*

The bh HPM-100-40 GaAsP hybrid detectors of the DCS-120 combine ultra-high sensitivity with the large active area of a PMT [4]. The large area avoids any alignment problems, and allows light to be efficiently collected through large pinholes and from the non-descanned beam path of the DCS-120 MP system [3]. In contrast to conventional PMTs or SPADs there is no secondary peak or ‘diffusion tail’ in the temporal response. Importantly, the hybrid detectors are free of afterpulsing. The absence of afterpulsing results in improved contrast, higher dynamic range of the decay curves recorded, and in the capability to obtain FCS data from a single detector. The combination of these features makes it easy to detect fluorescence from endogenous fluorophores in single cells and split the decay curves into several decay components, see Fig. 18.

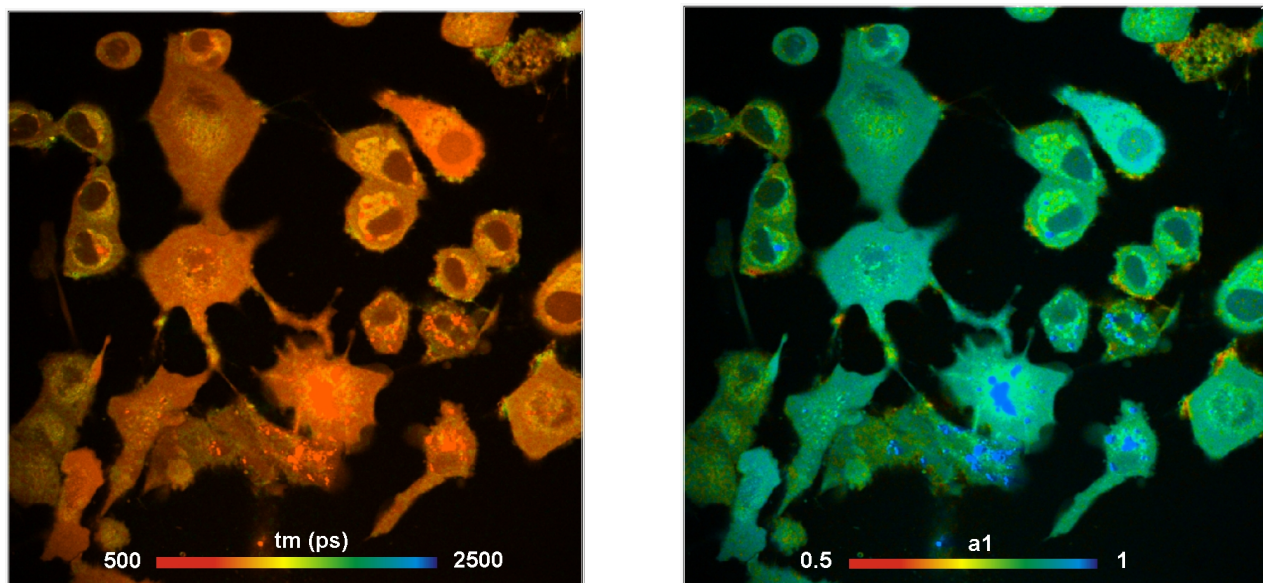


Fig. 18: Autofluorescence lifetime image of NADH in single cells. Lifetime image of mean lifetime of double exponential decay (left) and image of amplitude of fast decay component,  $a_1$  (right).

### *Sub-20 ps Time Resolution*

The DCS-120 system can be equipped with the new ultra-high speed HPM-100-06 and -07 hybrid detectors. The time resolution (IRF width) of these detectors is less than 20 ps, full width at half maximum [15]. Despite their slightly lower quantum efficiency these detectors deliver unprecedented accuracy for amplitudes and lifetimes of fast decay components of multi-exponential decay functions. The main application is metabolic imaging, where lifetimes and amplitude ratios of the decay components of NAD(P)H must be determined [16].

Fig. 19 shows NAD(P)H FLIM recorded with a DCS-120 MP multiphoton system. It shows an image of the mean lifetime,  $t_m$ , an image of the amplitude ratio,  $a_1/a_2$ , the system IRF, and a decay curve from the cursor position in the images.

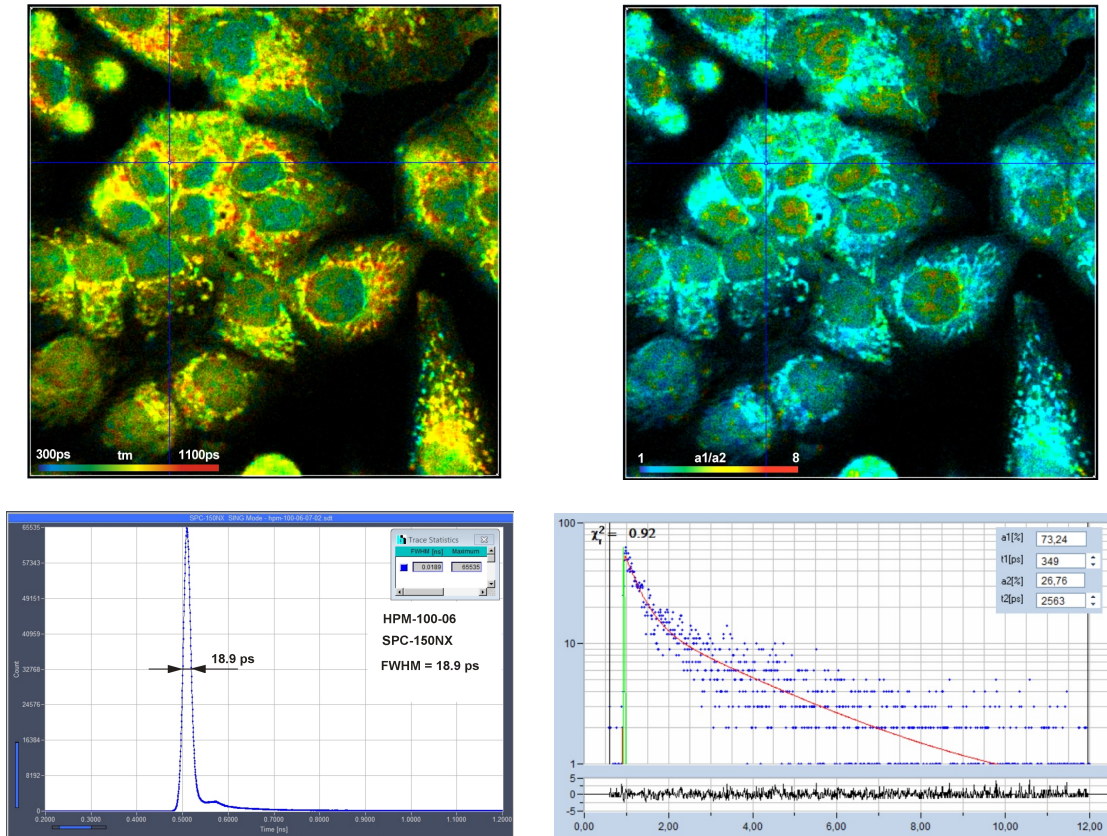


Fig. 19: NAD(P)H imaging of live cells. Image of the mean lifetime,  $t_m$ , image of the amplitude ratio,  $a_1/a_2$ , system IRF and decay curve at the cursor position.

## Precision Confocal-Detection FLIM

### High Time Resolution, Low Background

The pinhole of a confocal system not only suppresses out-of-focus fluorescence but also roomlight background and optical reflections. The decay data are therefore extraordinarily clean. Moreover, with the fast bh HPM-100-06 and -07 hybrid detectors the temporal instrument response function is essentially given by the laser pulse width. With the 375 nm, the 405 nm diode lasers the IRF width is less than 40 ps FWHM. A system IRF and a decay curve recorded with the HPM-100-06 and a diode laser are shown in Fig. 20. Please note the smooth residuals of the fit, an indication that the data are free of optical reflections.

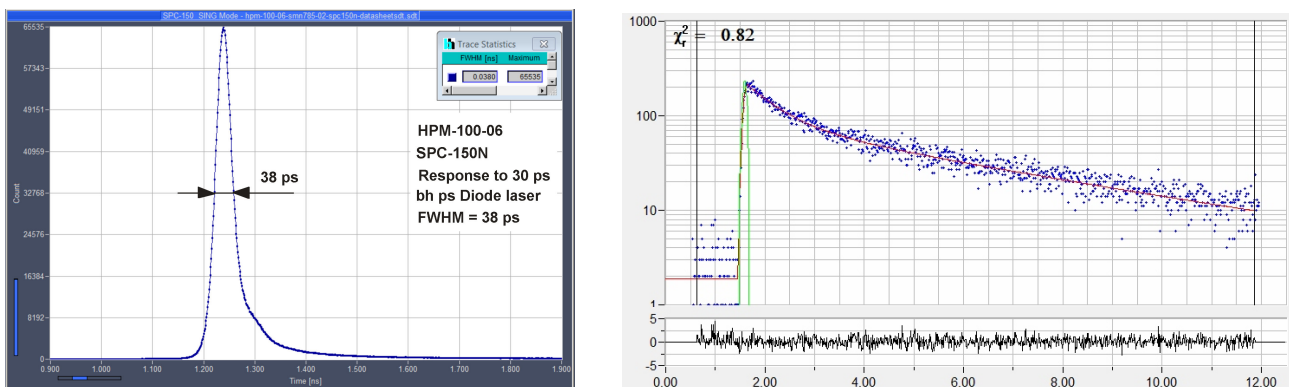


Fig. 20: Left: IRF with HPM-100-06 and bh 405 nm ps diode laser. Right: Fluorescence decay recorded with HPM-100-06 detector and bh 375 nm diode laser.

### Wide Range of Excitation Wavelengths

The DCS-120 confocal system can be used with a wide range of excitation wavelengths. Available diode-laser wavelengths range from 375 nm for excitation of NADH to 785 nm for excitation of NIR dyes. An NADH (autofluorescence) image is shown in Fig. 21, an image of a pig skin sample incubated with 3,3'-diethylthiatricarbocyanine in Fig. 22.

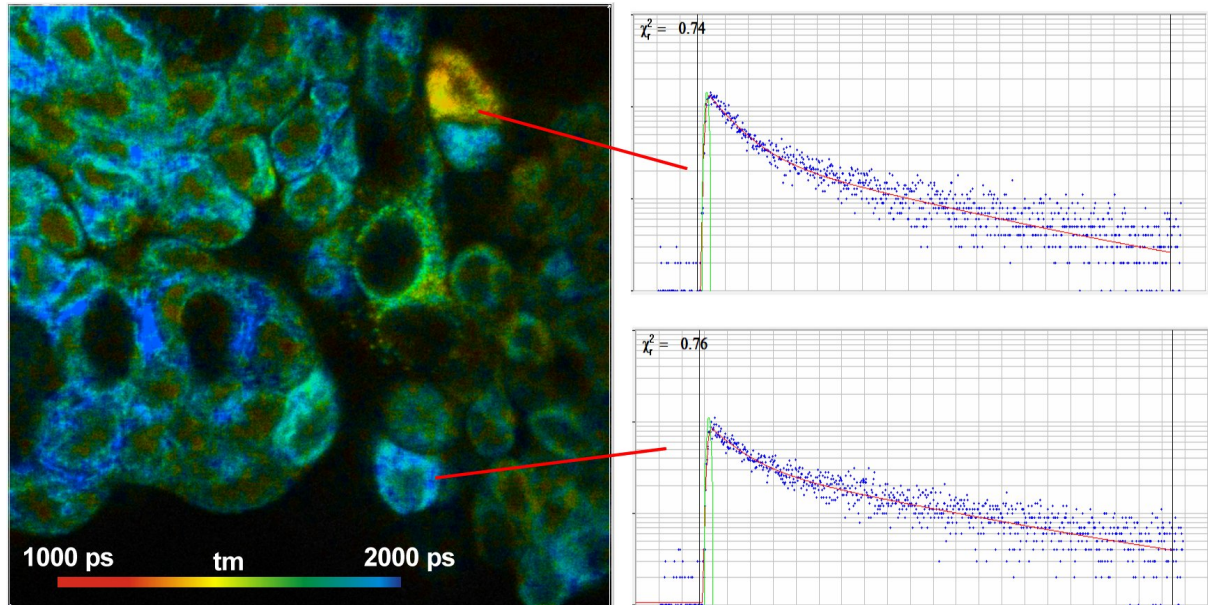


Fig. 21: UV-Excitation FLIM. NADH image of cells, excitation 370 nm, detection 420 to 475 nm.

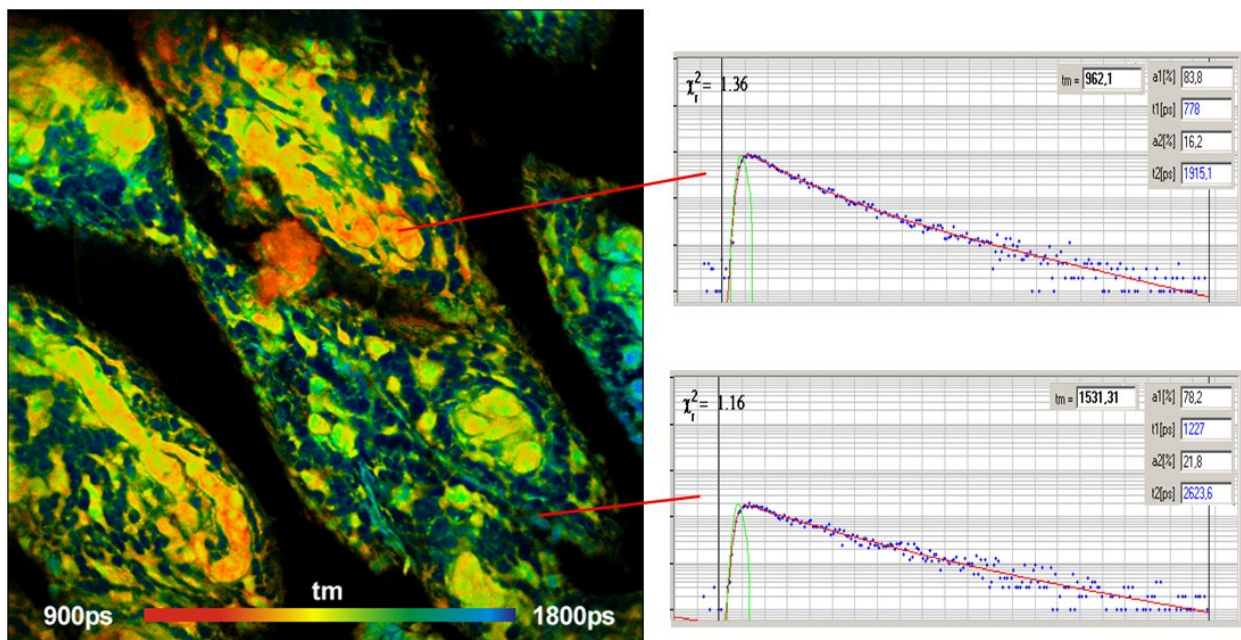


Fig. 22: Near-Infrared FLIM. Pig skin sample stained with 3,3'-diethylthiatricarbocyanine, detection wavelength, excitation 690 nm, detection wavelength from 780 nm to 900 nm.

In the DCS-120 WB wideband version lasers can be swapped without the need of re-alignment. The wideband system can even be used with tuneable excitation. Images obtained with a Toptica Ichrome laser [55] are shown in Fig. 23.

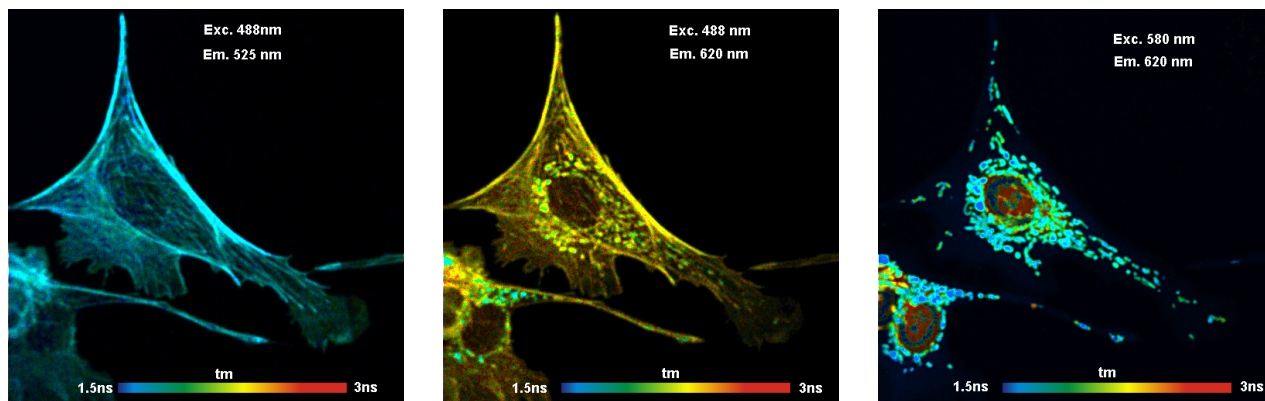


Fig. 23: Tuneable excitation with DCS-120 WB and Toptica Ichrome laser. Left to right: Excitation 488 nm emission  $525 \pm 15$  nm, excitation 488 nm emission  $620 \pm 30$  nm, and excitation 580 nm emission  $620 \pm 30$  nm.

### *Autofluorescence FLIM of Small Organisms*

The wide range of excitation and detection wavelengths and the high sensitivity makes the DCS-120 an excellent system for autofluorescence FLIM of small organisms. Fig. 24 shows an autofluorescence image of *Artemia salinas*, a small shrimp living in briny water. The excitation wavelength was 405 nm, the detection wavelength from 420 nm to 560 nm.

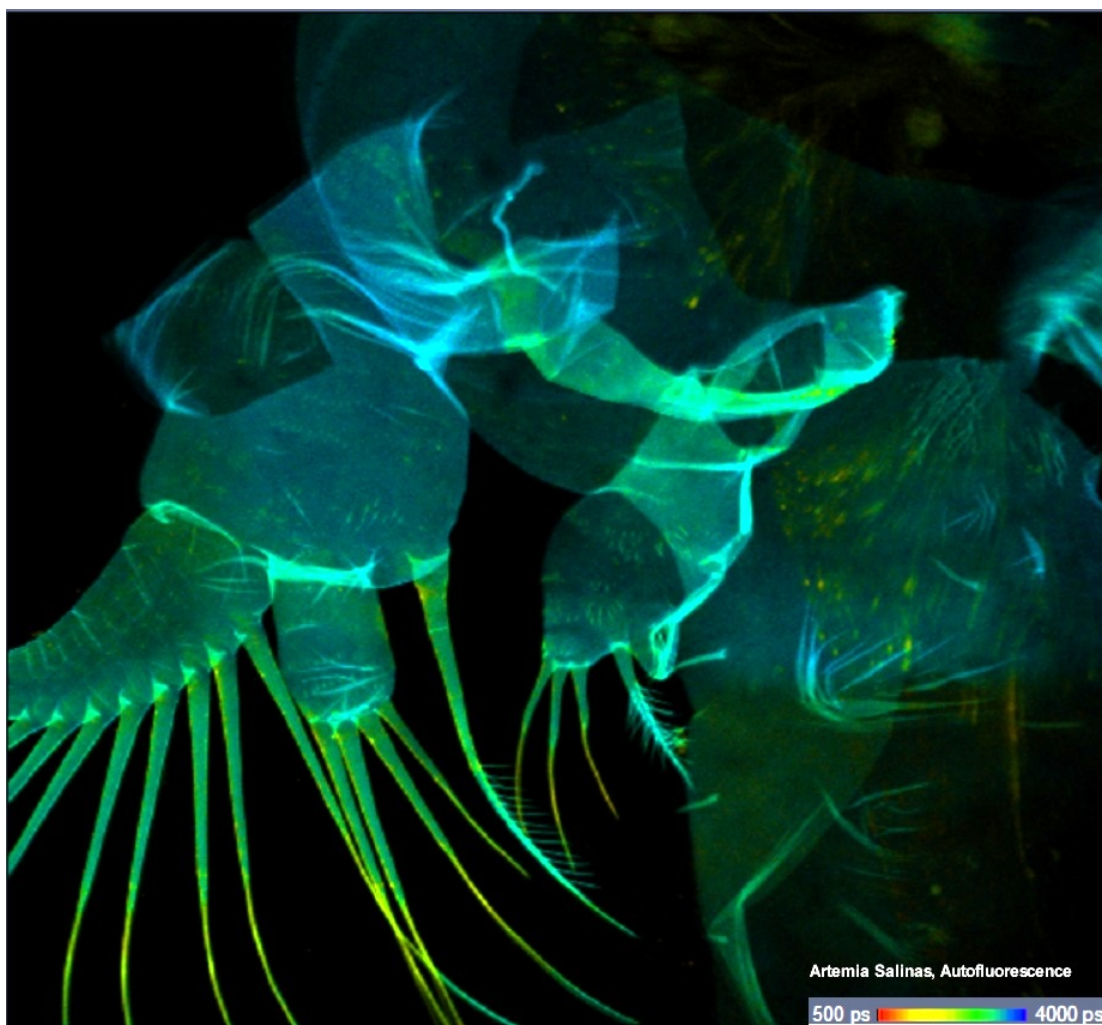


Fig. 24: Autofluorescence FLIM of *Artemia salinas*, DCS-120 confocal system with HPM-100-40 hybrid detectors and SPC-180 TCSPC modules

### Laser Wavelength Multiplexing

The two ps-diode lasers of the DCS-120 system can be multiplexed on a pixel-by-pixel, line-by-line, or frame-by-frame basis. With the two lasers and the two detection channels of the DCS system, images for three or four combinations of excitation and emission wavelength are obtained. An example is shown in Fig. 25.

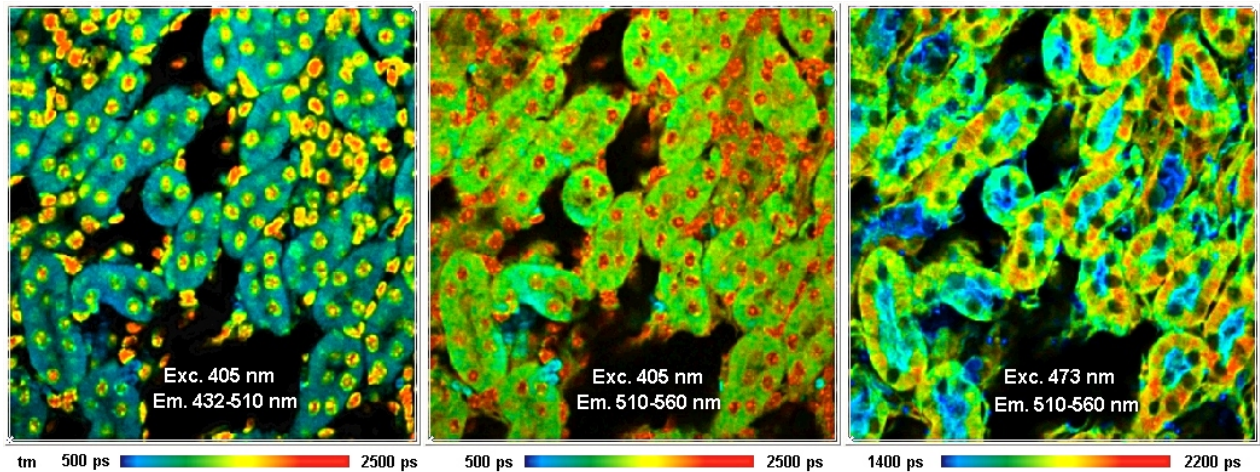


Fig. 25: Excitation wavelength multiplexing, 405 nm and 473 nm. Detection wavelength 432 nm to 510 nm and 510 nm to 550 nm. Mouse kidney section, stained with Alexa 488 WGA, Alexa 568 phalloidin, and DAPI.

The most frequent application of excitation wavelength multiplexing is metabolic FLIM, where NAD(P)H and FAD data have to be acquired simultaneously, see [3, 31]. NADH and FAD Images recorded by multiplexed excitation is shown in Fig. 26.

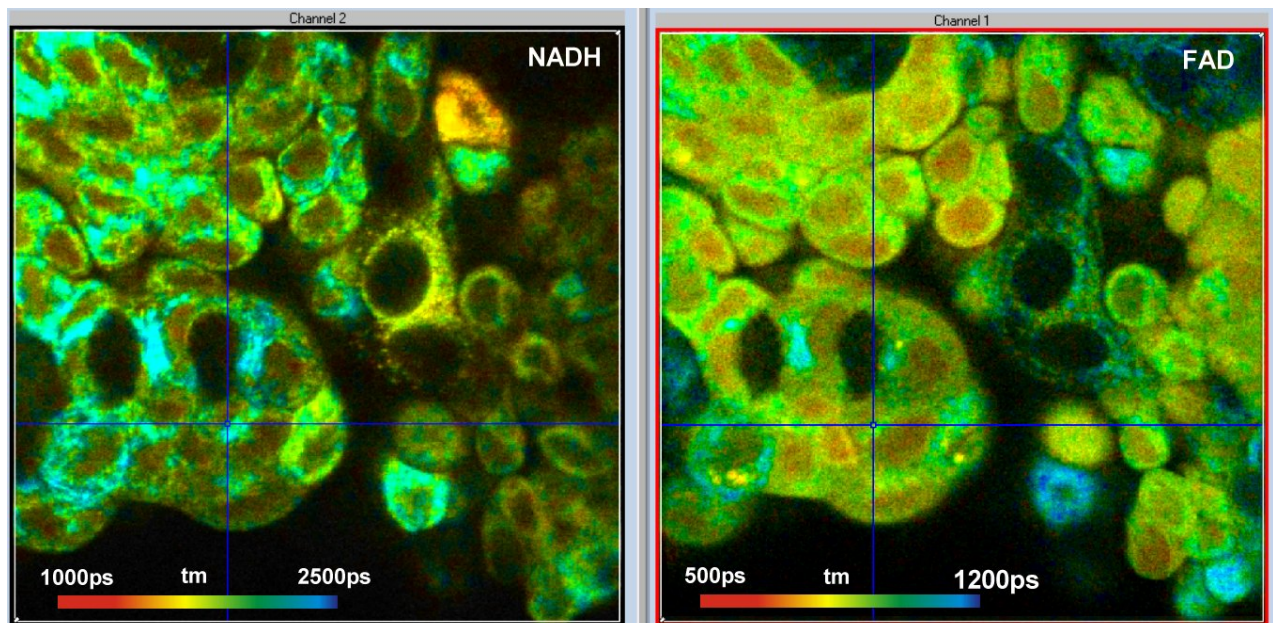


Fig. 26: Laser-multiplexed FLIM of NADH and FAD

## Multiphoton FLIM

### DCS-120 MP: Multiphoton FLIM with Ti:Sa or Femtosecond Fibre Laser

Multiphoton FLIM is used when images from deep layers of biological tissue have to be imaged. A two-photon FLIM image of *Artemia salinas* (a small shrimp) recorded by the DCS-120 MP system is shown in Fig. 27. The image was recorded with the Femto-Fibre-Pro (fibre-laser version) of the DCS-120 MP [21].

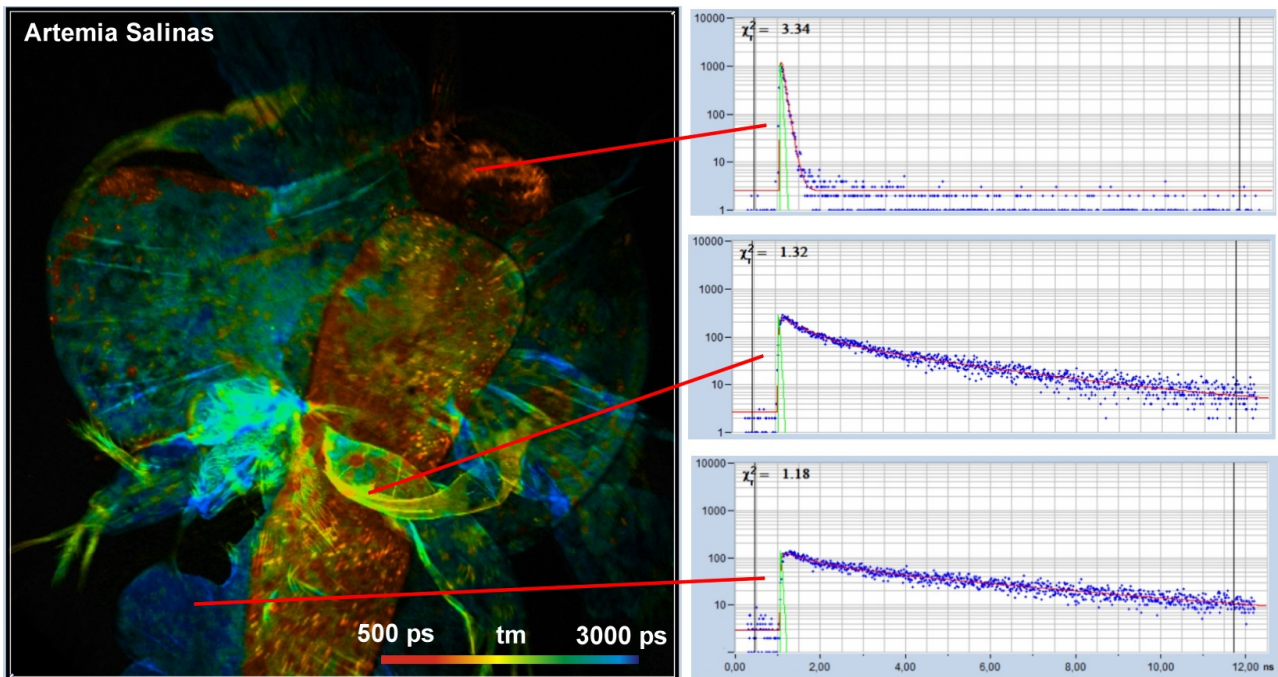


Fig. 27: Autofluorescence FLIM image of *Artemia salinas*, a brine shrimp. Mean (amplitude-weighted) lifetime of double-exponential decay. Decay functions of selected areas shown on the right.

FLIM images of pig skin in different depth of the tissue are shown in Fig. 28. The images were recorded by a DCS-120 MP with a Ti:Sa-Laser.

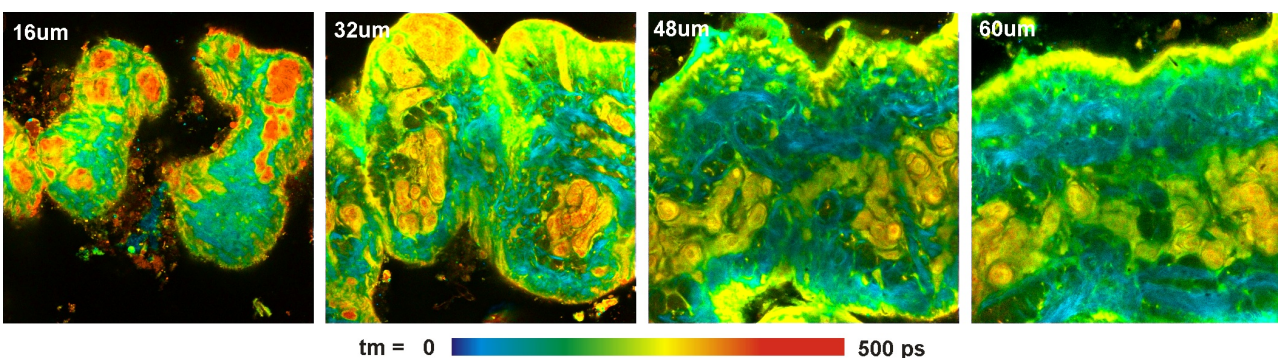


Fig. 28: Pig skin, autofluorescence, image in different depth in the sample. Amplitude-weighted lifetime of triple-exponential decay model

The detectors for the NDD ports are the same as for the confocal ports. DCS systems with two TCSPC channels can be equipped with two non-descanned and two confocal detectors, either pair being active at a time.

### Multiphoton NADH FLIM with Ultra-Fast Detectors

In combination with the ultra-fast HPM-100-06 and -07 detectors, the DCS-120 MP multiphoton system achieves an instrument response function (IRF) of less than 20 ps FWHM [15, 31]. The fast response greatly improves the accuracy at which fast decay components can be extracted from a multi-exponential decay. Applications are mainly in the field of metabolic FLIM, which requires separation of the decay components bound and unbound NADH [16]. An NADH FLIM image recorded with the DCS-120 MP using an HPM-100-06 is shown in Fig. 29.

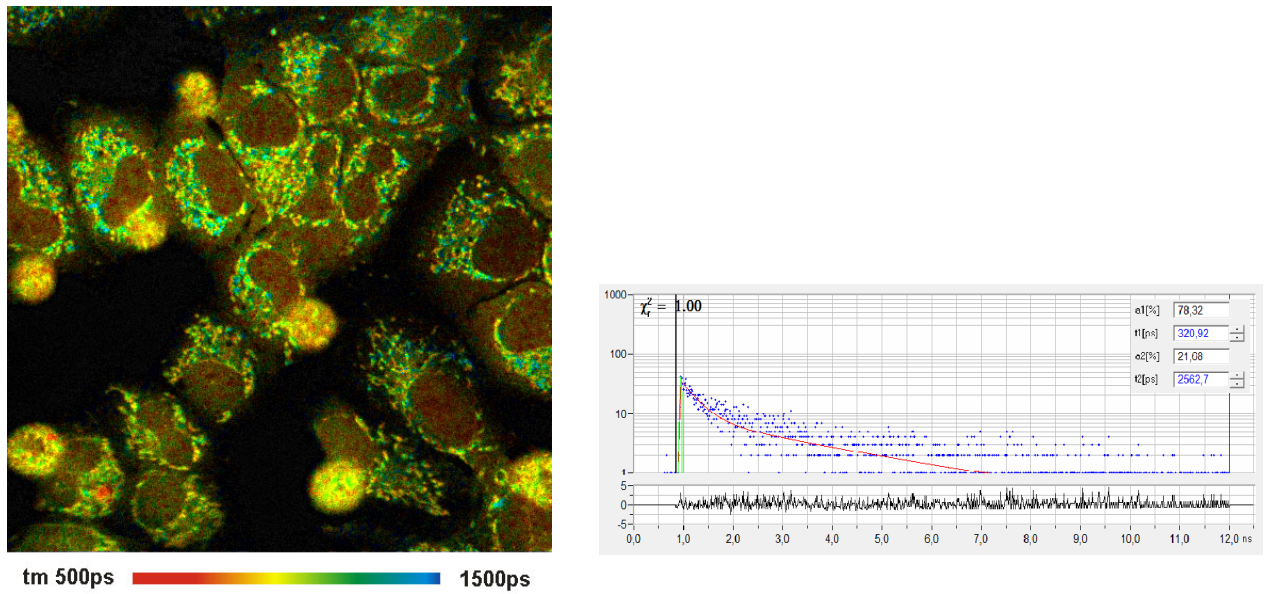


Fig. 29: Left: NADH Lifetime image, amplitude-weighted lifetime of double-exponential fit. Right: Decay curve in selected spot, 9x9 pixel area. DCS-120 MP with HPM-100-06 detector and SPC-160 TCSPC/FLIM module, FLIM data format 512x512 pixels, 1024 time channels.

### FLIM of Ultra-Fast Fluorescence-Decay Processes in Biological Material

Due to the short pulse width of the femtosecond lasers the DCS-120 MP system delivers extremely high temporal resolution. An example is shown in Fig. 30. The image shows mushroom spores of *Boletus edulis* []. The image was recorded by a DCS-120 MP with a Femto-Fibre-Pro laser (Toptica), ultra-fast HPM-100-06 detectors, and SPC-150NX TCSPC modules. The data show clearly a decay component of 20 ps lifetime.

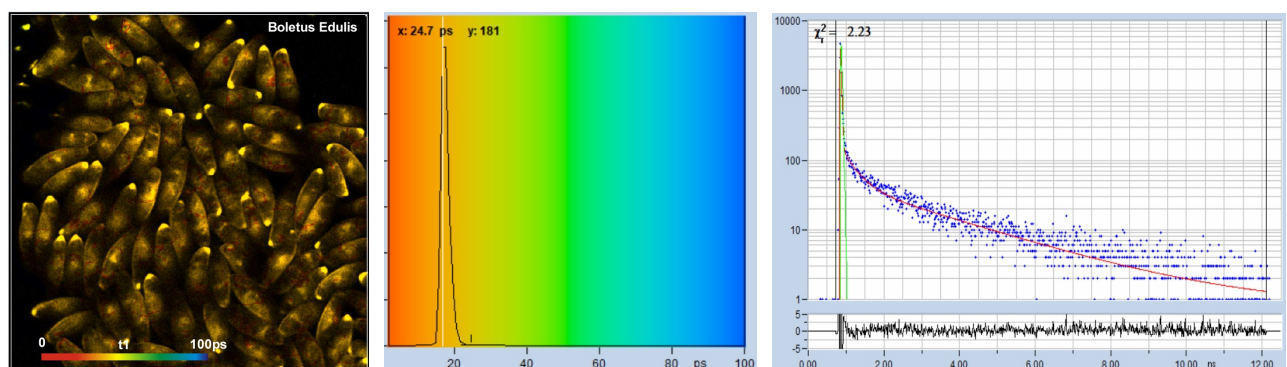


Fig. 30: Spores of *Boletus edulis*. Left to right: Image of fast decay component,  $t_1$ , of triple-exponential decay model, histogram of  $t_1$ , and decay curve in selected spot. Data from [36].

## *Integrated Control of Ti:Sa Laser and AOM*

The control of the Ti:Sa laser and the AOM (acousto-optical modulator) of DCS-120 MP Multiphoton systems is integrated in the SPCM software. Both the laser wavelength and the laser power are controlled from the ‘Ti:Sa Laser and AOM Control’ panel of the software. The AOM is automatically tuned to the same wavelength as the laser.

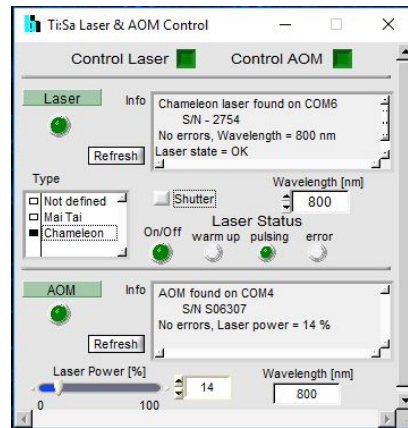


Fig. 31: Ti:Sa Laser and AOM control panel

## Advanced Functions for FLIM in Life Sciences

### Metabolic FLIM

The DCS-120 Metabolic FLIM system is based on simultaneous recording of lifetime images of NAD(P)H (nicotinamide adenine (pyridine) dinucleotide) and FAD (flavin adenine dinucleotide). The metabolic FLIM system uses laser wavelength multiplexing to simultaneously record lifetime images of the two fluorophores. By multi-exponential decay analysis of the NADH and FAD signals, the system delivers information on the metabolic state of the cells or the tissue investigated. Please see [3, 31].

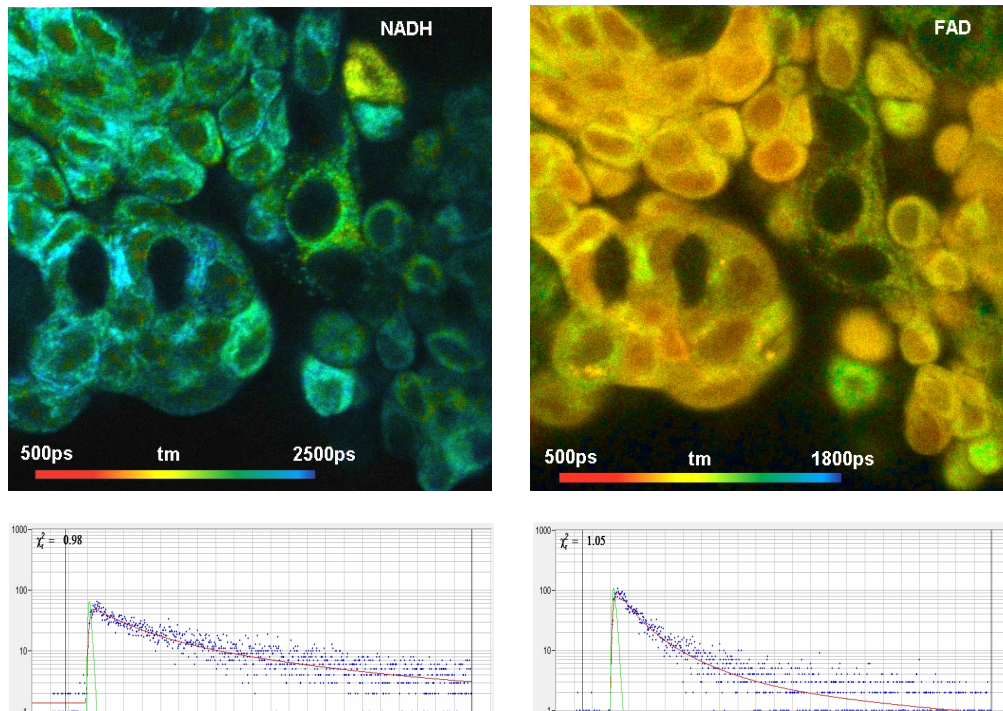


Fig. 32: NADH and FAD images, recorded simultaneously by the DCS-120 metabolic-FLIM system

In metabolic FLIM, the primary information is not in the mean lifetime,  $t_m$ , but in the amplitudes of the decay components,  $a_1$  and  $a_2$ . Due to its superior photon efficiency and time resolution the DCS-120 metabolic FLIM system provides such images at unprecedented accuracy. An example is shown in Fig. 33.

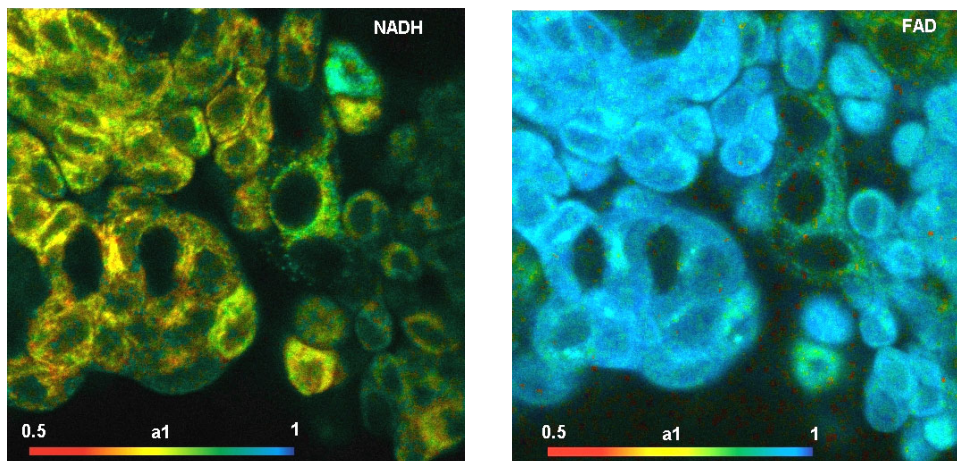


Fig. 33: NADH and FAD images, showing the amplitude of the fast decay component,  $a_1$ .

**Multi-Wavelength FLIM**

With the bh multispectral FLIM detectors the DCS-120 records FLIM simultaneously in 16 wavelength channels [23, 26, 31]. The images are recorded by a multi-dimensional TCSPC process which uses the wavelength of the photons as a coordinate of the photon distribution. There is no time gating, no wavelength scanning and, consequently, no loss of photons in this process. The system thus reaches near-ideal recording efficiency. Moreover, dynamic effects in the sample or photobleaching do not cause distortions in the spectra or decay functions. Multi-wavelength FLIM got an additional push from the new 64-bit SPCM software, and from the introduction of a highly efficient GaAsP multi-wavelength detector. 64-bit software works with enormously large photon distributions, and the GaAsP detector delivers the efficiency to fill them with photons. As a result, 16 images in 16 wavelength channels can be recorded at a resolution of 512x512 pixels and 256 time channels. An example is shown in Fig. 34.

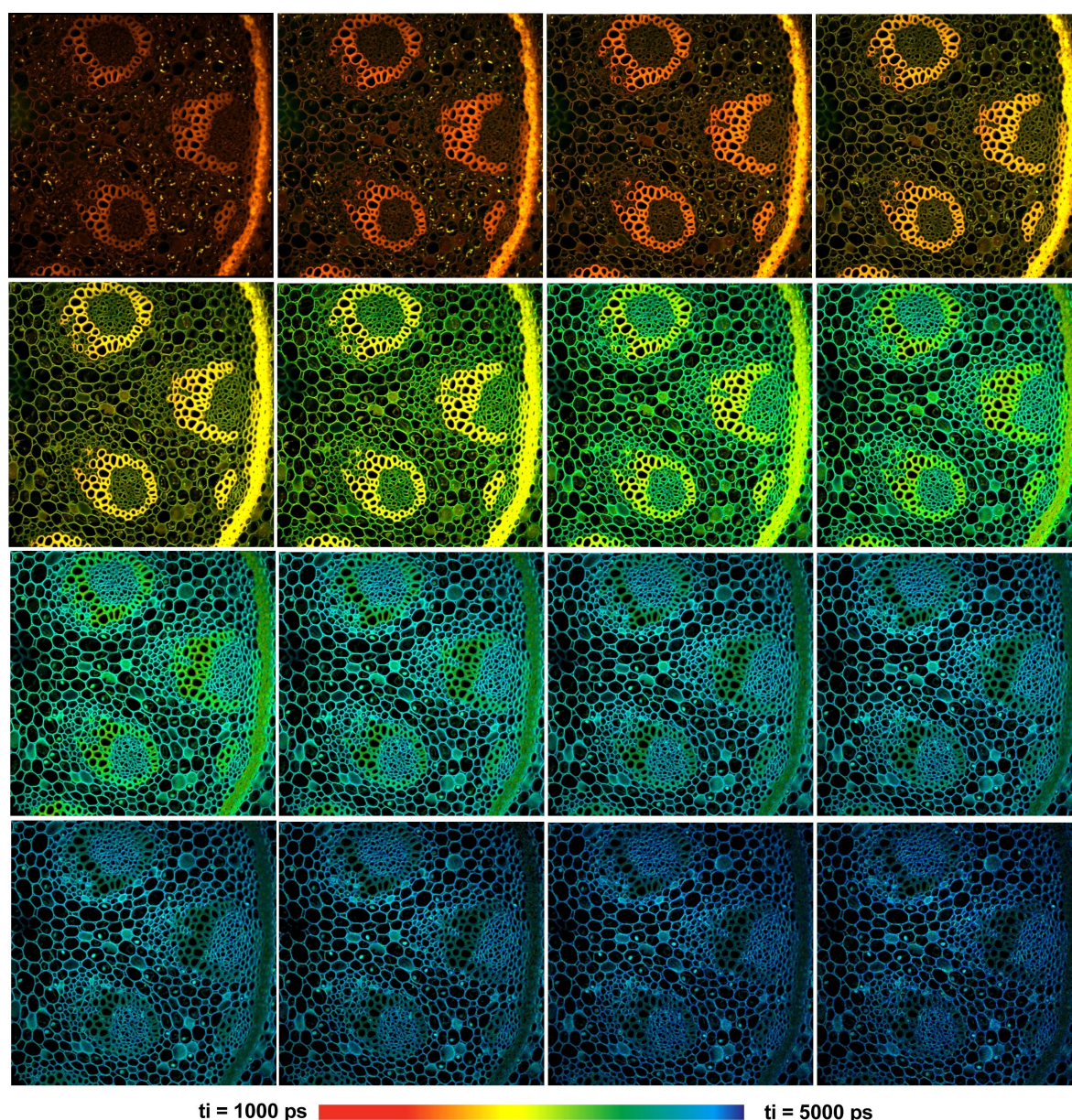


Fig. 34: Multi-wavelength FLIM with the bh MW-FLIM GaAsP 16-channel detector. 16 images with 512 x 512 pixels and 256 time channels were recorded simultaneously. Wavelength from upper left to lower right, 490 nm to 690 nm, 12.5 nm per image. DCS-120 confocal scanner, Zeiss Axio Observer microscope, x20 NA=0.5 air lens.

Fig. 35 demonstrates the true spatial resolution of the data. Images from two wavelength channels, 502 nm and 565 nm, were selected from the data shown Fig. 34, and displayed at larger scale and with individually adjusted lifetime ranges. With 512x512 pixels and 256 time channels, the spatial and temporal resolution of the individual images is comparable with what previously could be reached for FLIM at a single wavelength. Decay curves for selected pixels of the images are shown in Fig. 36.

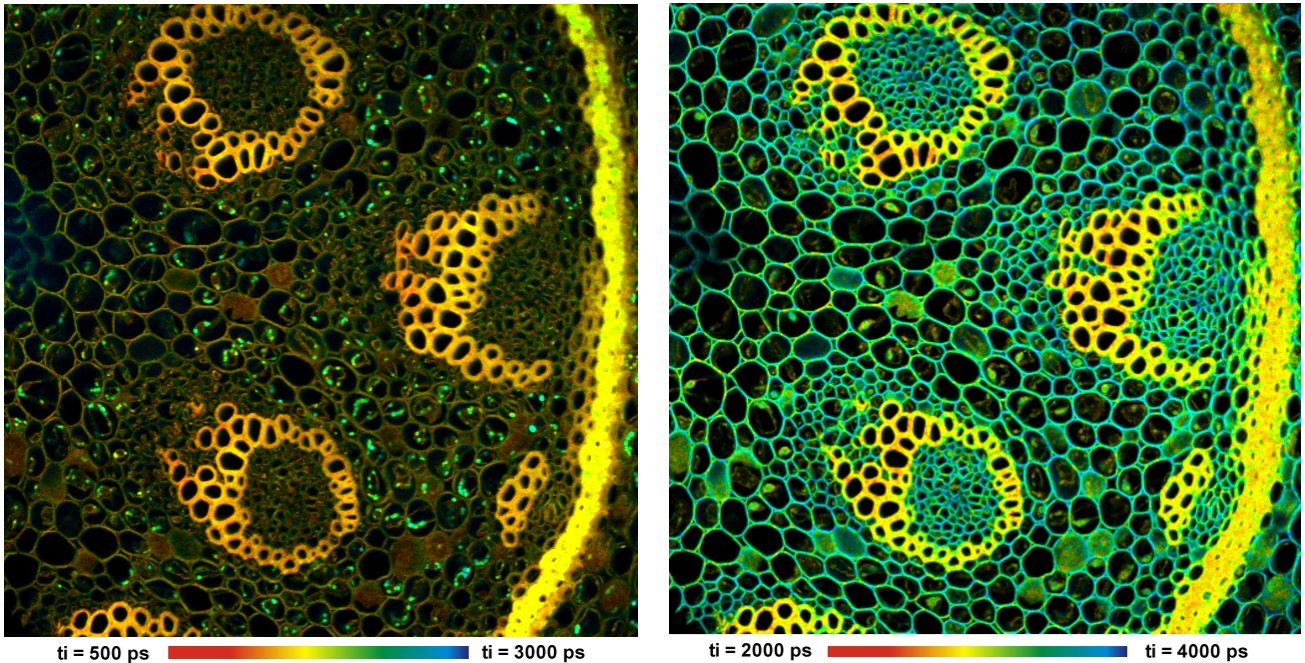


Fig. 35: Two images from the array shown in Fig. 34, displayed in larger scale and with individually adjusted lifetime range. Wavelength channels 502 nm (left) and 565 nm (right). The images have 512 x 512 pixels and 256 time channels.

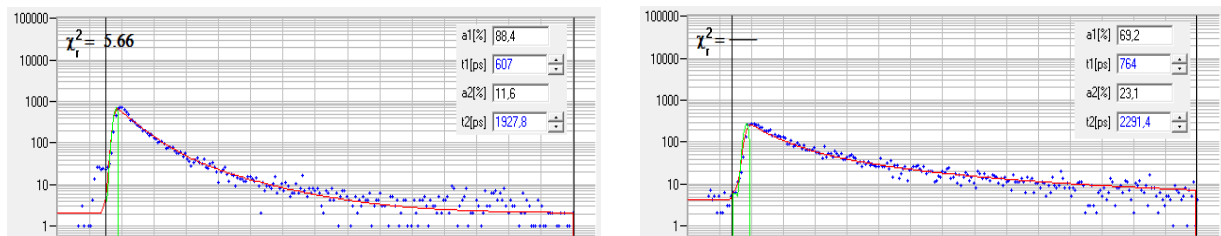


Fig. 36: Decay curves at selected pixel position in the images shown above. Blue dots: Photon numbers in the time channels. Red curve: Fit with a double-exponential model.

### ***Z Stack Recording by Record-and-Save Procedure***

In combination with the Zeiss Axio Observer Z1 microscope the DCS-120 system is able to record z-stacks of FLIM images. The sample is continuously scanned. For each plane, a FLIM image is acquired for a specified ‘collection time’. Then the data are saved in a file, the microscope is commanded to step to the next plane, and the next image is acquired. The procedure continues for a specified number of Z planes. A Z stack of autofluorescence images taken at a water flea is shown in Fig. 37.

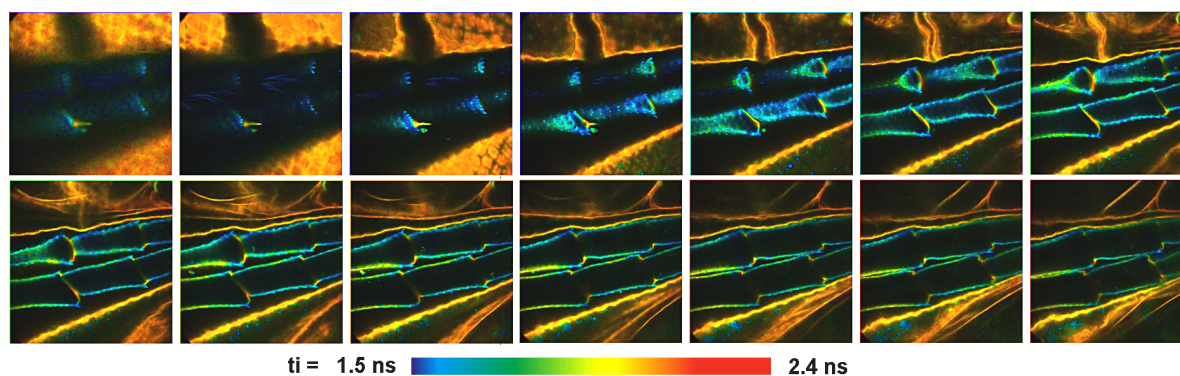


Fig. 37: Z stack recording, part of a water flea, autofluorescence. 14 steps in Z, step width 4  $\mu\text{m}$ .

### *Z-Stack recording by Mosaic FLIM*

Z Stacks of FLIM images can be recorded by the Mosaic FLIM function of the 64 bit SPCM software. As the microscope scans consecutive images planes in the sample the FLIM system records the data into consecutive elements of a FLIM mosaic. The advantage over the traditional record-and-save procedure is that no time has to be reserved for save operations, and that the entire array can be analysed in a single analysis run.

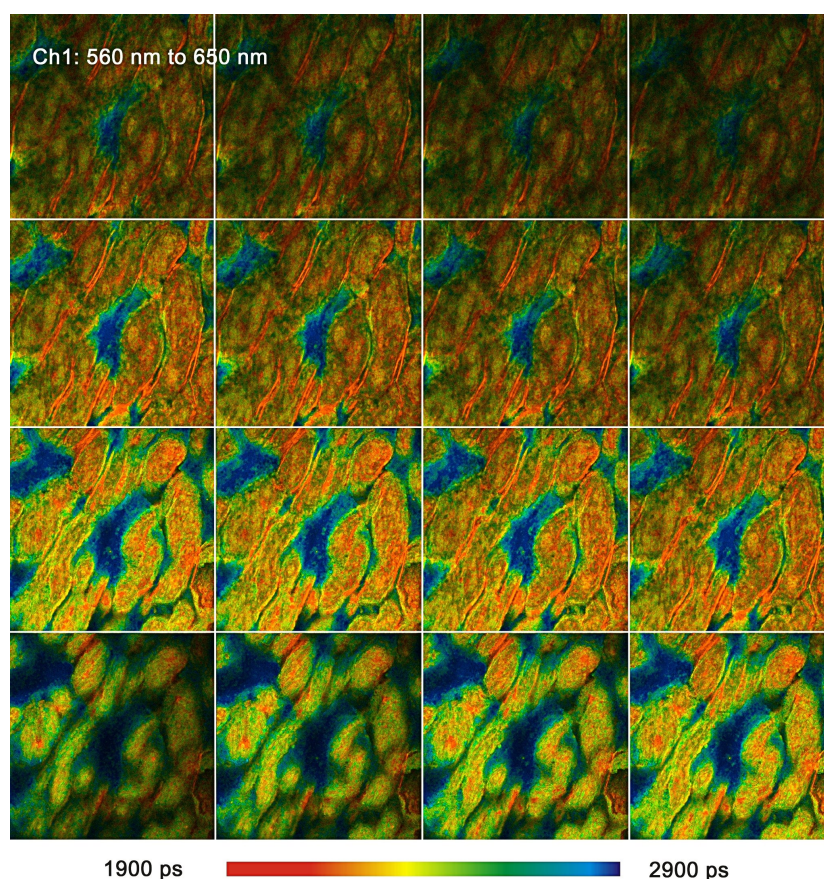


Fig. 38: FLIM Z-stack, recorded by Mosaic FLIM. Pig skin, autofluorescence. 16 planes, 0 to 30  $\mu\text{m}$  from top of the tissue. Each element of the FLIM mosaic has 512x512 pixels and 256 time channels per pixel.

### *Time-Series FLIM by Record-and-Save Procedure*

Time-series FLIM by the traditional record-and-save procedure is available for all DCS-120 system versions. With the SPC-152 dual-channel systems time series as fast as 2 images per second can be

obtained [58]. A time series taken at a moss leaf is shown in Fig. 39. The fluorescence lifetime of the chloroplasts changes due to the Kautski effect induced by the illumination.

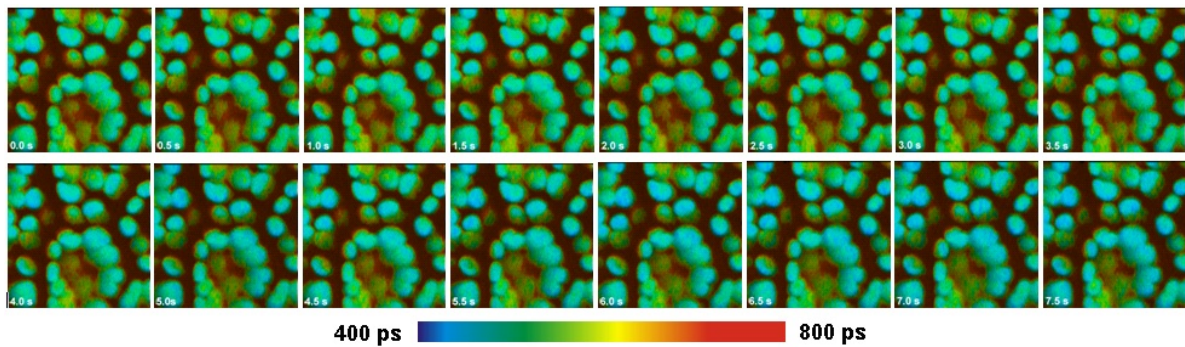


Fig. 39: Time-series FLIM, 2 images per second. Chloroplasts in a leaf, the fluorescence lifetime of the chlorophyll decreases with the time of exposure.

### *Recording of Dynamic Effects by Mosaic FLIM*

SPCM 64-bit software versions later than 2014 have a ‘Mosaic Imaging’ function implemented. For time-series recording, subsequent frames of the scan are recorded into subsequent elements of the mosaic. The sequence can be repeated and accumulated [31, 34]. The time per mosaic element can be as short as a single frame, which can be less than 100 ms. Another advantage is that the entire array can be analysed in a single SPCImage data analysis run. Fig. 40 shows the change of the lifetime of chlorophyll in plant tissue with the time of illumination.

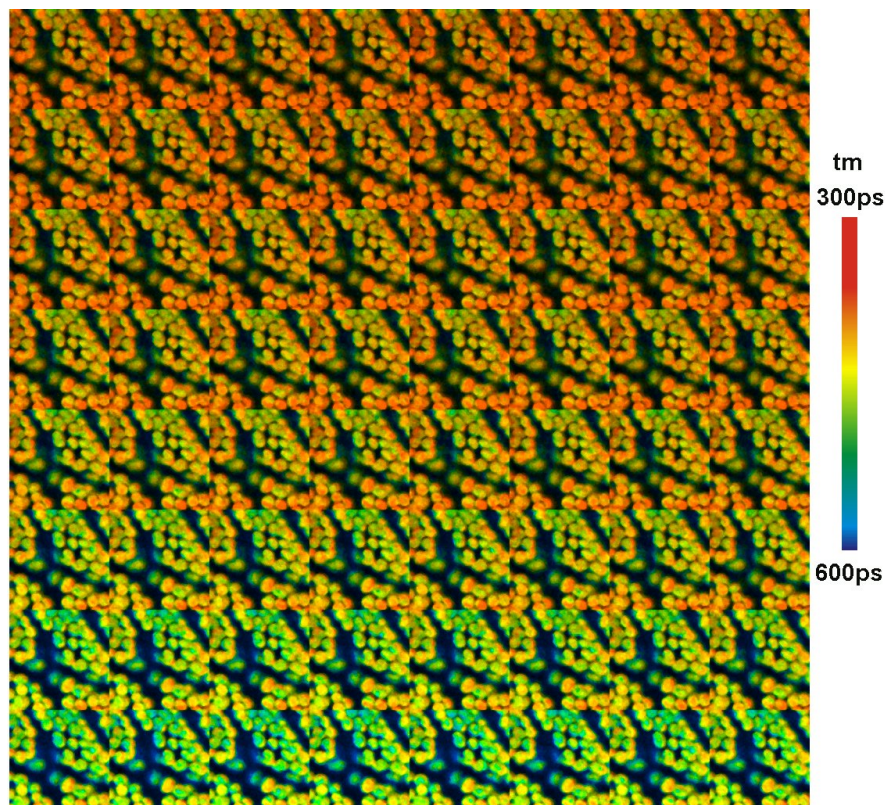


Fig. 40: Time series of chloroplasts in a leaf recorded by Mosaic Imaging. 64 mosaic elements, each 128x128 pixels, 256 time channels. Scan time per element 1s. Experiment time from lower left to upper right. Amplitude-weighted lifetime of double-exponential decay.

**FLITS: Fluorescence Lifetime-Transient Scanning**

FLITS records dynamic effects in the fluorescence lifetime of a sample along a one-dimensional scan. The technique is based on building up a photon distribution over the distance along the scan, the arrival times of the photons after the excitation pulses, and the experiment time after a stimulation of the sample. The maximum resolution at which lifetime changes can be recorded is given by the line scan time. With repetitive stimulation and triggered accumulation transient lifetime effects can be resolved at a resolution of about one millisecond [31, 32].

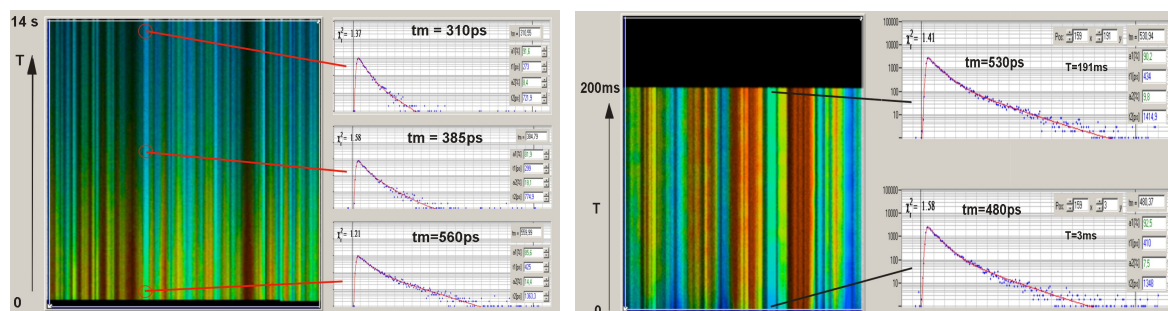


Fig. 41: FLITS of chloroplasts in a grass blade, change of fluorescence lifetime after start of illumination. Left: Non-photochemical transient, transient resolution 60 ms. Right: Photochemical transient. Triggered accumulation, transient resolution 1 ms.

The technique has been used to record  $Ca^{++}$  transients in live neurons at a resolution of 2 ms, see [54].

**Simultaneous FLIM/PLIM**

Phosphorescence and fluorescence lifetime images are recorded simultaneously by bh’s proprietary FLIM/PLIM technique. The technique is based on modulating a ps diode laser synchronously with the pixel clock of the scanner [28, 31]. FLIM is recorded during the ‘On’ time, PLIM during the ‘Off’ time of the laser. The SPCM software delivers separate images for the fluorescence and the phosphorescence which are then analysed with SPCImage FLIM/PLIM analysis software. Please see [3] for details.

Currently, there is increasing interest in PLIM for background-free recording and for oxygen sensing [1, 2, 44, 45, 56, 67, 80]. In these applications, the bh technique delivers a far better sensitivity than PLIM techniques based on single-pulse excitation. The real advantage of the FLIM/PLIM technique used in the DCS-120 is, however, that FLIM and PLIM are obtained *simultaneously*. It is thus possible to record metabolic information via FLIM of the NADH and FAD fluorescence, and simultaneously map the oxygen concentration via PLIM. An example is shown in Fig. 42.

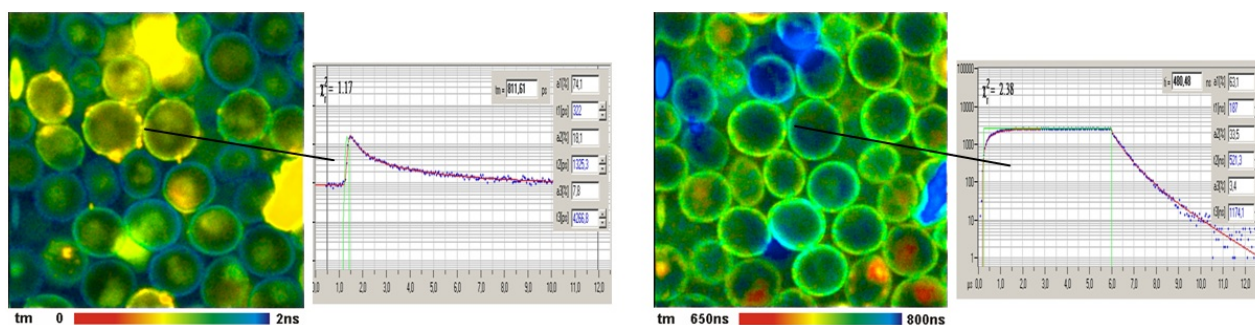


Fig. 42: Yeast cells stained with (2,2'-bipyridyl) dichlororuthenium (II) hexahydrate. FLIM and PLIM image, decay curves in selected spots.

PLIM can also be interesting for the investigation the luminescence properties of inorganic compounds, see Fig. 43. A typical example is the study of migration, possible dissolution, and chemical reaction of nanoparticles from sunscreens in skin. The results of such studies are highly important to skin cancer research.

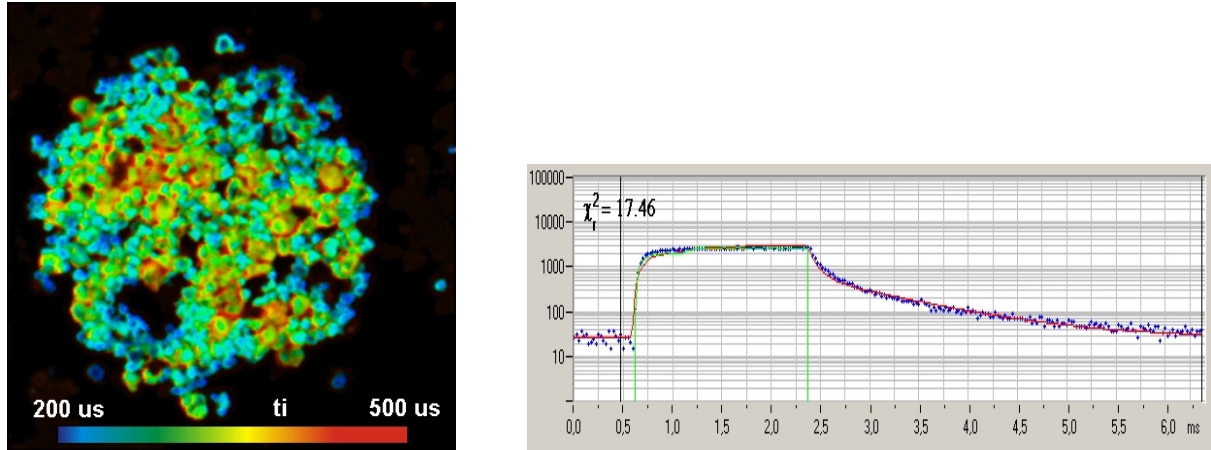


Fig. 43: Phosphorescence lifetime imaging of nanoparticles, here of the phosphor of a cathode-ray tube. Left: Lifetime image. Right: Phosphorescence decay curve at selected position within the image

## Imaging of Macroscopic Objects - The DCS-120 MACRO System

### *FLIM of cm-Size Objects*

The DCS MACRO version of the DCS system scans objects directly in the focal plane of the scanner. Objects up to a size of 12 mm can be imaged at high resolution. Please see [3, 31, 75].

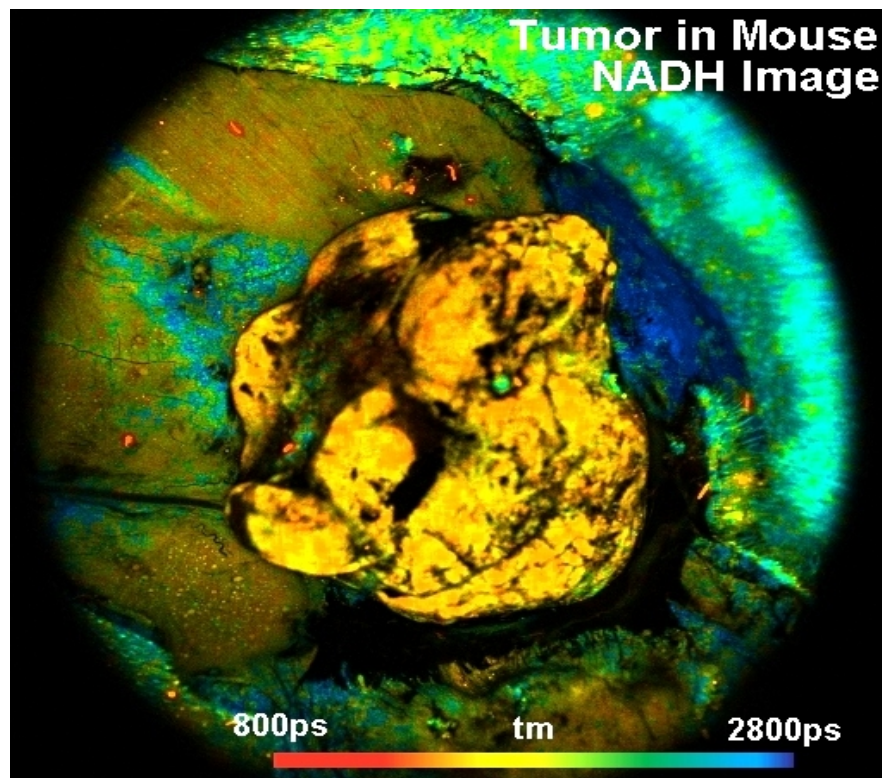


Fig. 44: Lifetime Images of tumor in a mouse. NADH image, recorded by the DCS-120 Macro system.

### DCS Macro with Motor Stage

The image area of the DCS MACRO can be extended by a motorised sample stage. Mosaic FLIM is used to record images of objects with dimensions in the 10-cm range, see Fig. 45.

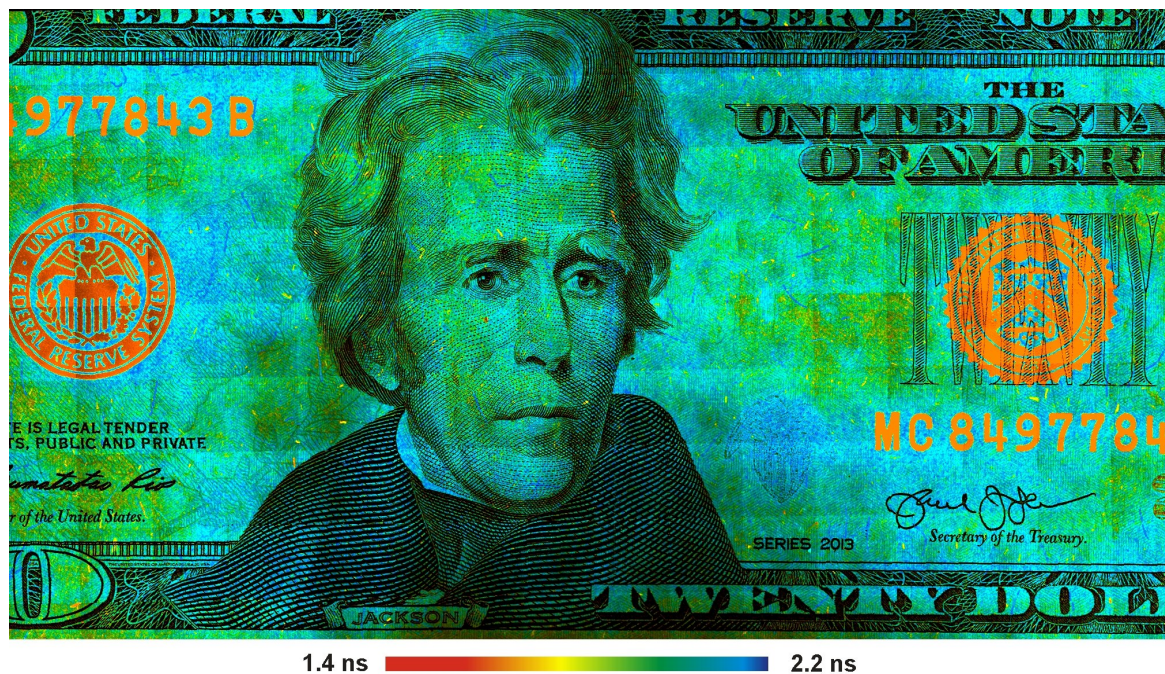


Fig. 45: Mosaic FLIM image of a \$20 bill. Combination of beam scanning with sample stepping by motor stage.

### FLIM through Endoscopes

The DCS-120 Macro can be combined with endoscopes. Optical details are described in [3] and [31]. Images of (benign) human skin lesions are shown in Fig. 46.

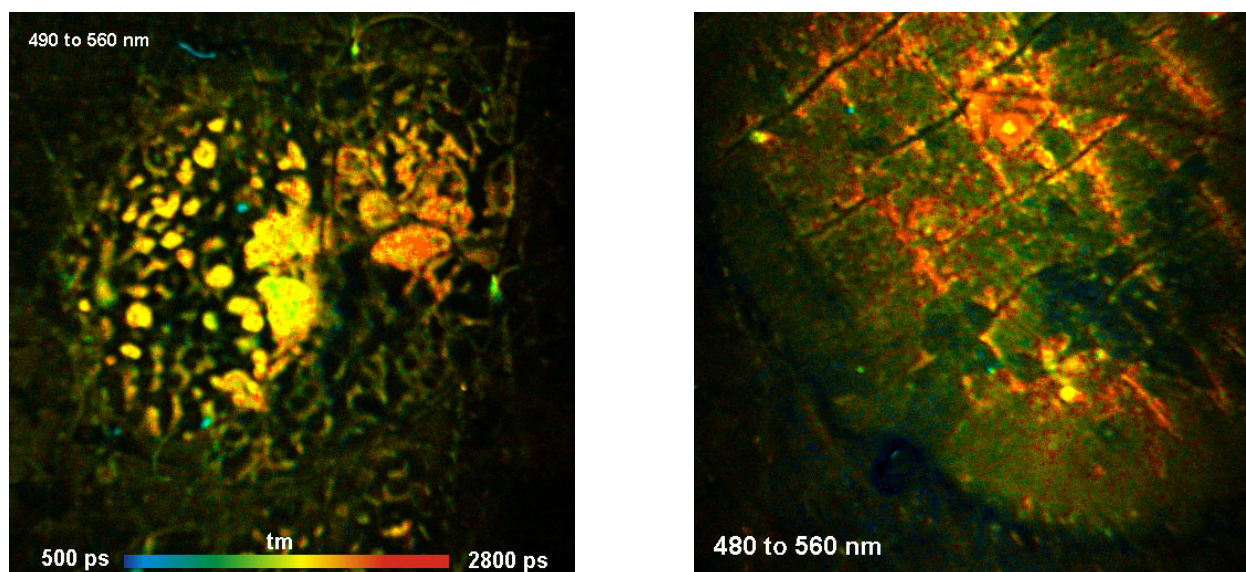


Fig. 46: Basal cell papilloma (left) and a keratocystic lesion (right), scanned in vivo through a rigid endoscope. Excitation wavelength 405 nm, detection wavelength 480 to 560 nm. Excitation power 50  $\mu$ W, acquisition time 10 seconds.

## FCS

The bh GaAsP hybrid detectors deliver highly efficient FCS. Because the detectors are free of afterpulsing there is no afterpulsing peak in autocorrelation data [4]. Thus, accurate diffusion times and molecule parameters are obtained from a single detector. Compared to cross-correlation of split signals, correlation of single-detector signals yields a four-fold increase in correlation events. The result is a substantial improvement in the SNR of FCS recordings.

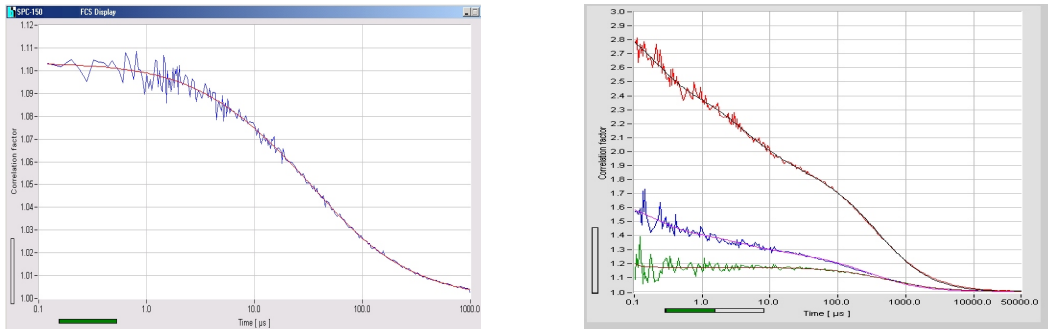


Fig. 47: FCS curve recorded by a single HPM-100 detector. There is no afterpulsing peak, and the efficiency is four times higher than for commonly used cross-correlation of split light signals. Right: Dual-colour FCS, autocorrelation blue and red, cross-correlation green. Online fit with FCS procedures of SPCM data acquisition software.

## SPCImage NG FLIM Data Analysis

SPCImage NG is a new generation of bh's TCSPC-FLIM data analysis software. It combines time-domain and frequency-domain analysis, uses a maximum-likelihood (MLE) algorithm to calculate the parameters of the decay functions in the individual pixels, and accelerates the analysis procedure by GPU processing. 1D and 2D parameter histograms are available to display the distribution of the decay parameters over the pixels of the image or over selectable ROIs. Image segmentation can be performed via the phasor plot. Pixels with similar phasor signature can be combined for high-accuracy time-domain analysis. SPCImage NG provides decay models with one, two, or three exponential components, incomplete-decay models, and shifted-component models. Another important feature is advanced IRF modelling, making it unnecessary to record IRFs for the individual FLIM data sets. For detailed description please see [3, 31] and SPCImage NG Overview Brochure [20]. A typical main panel of SPCImage NG is shown in Fig. 48.

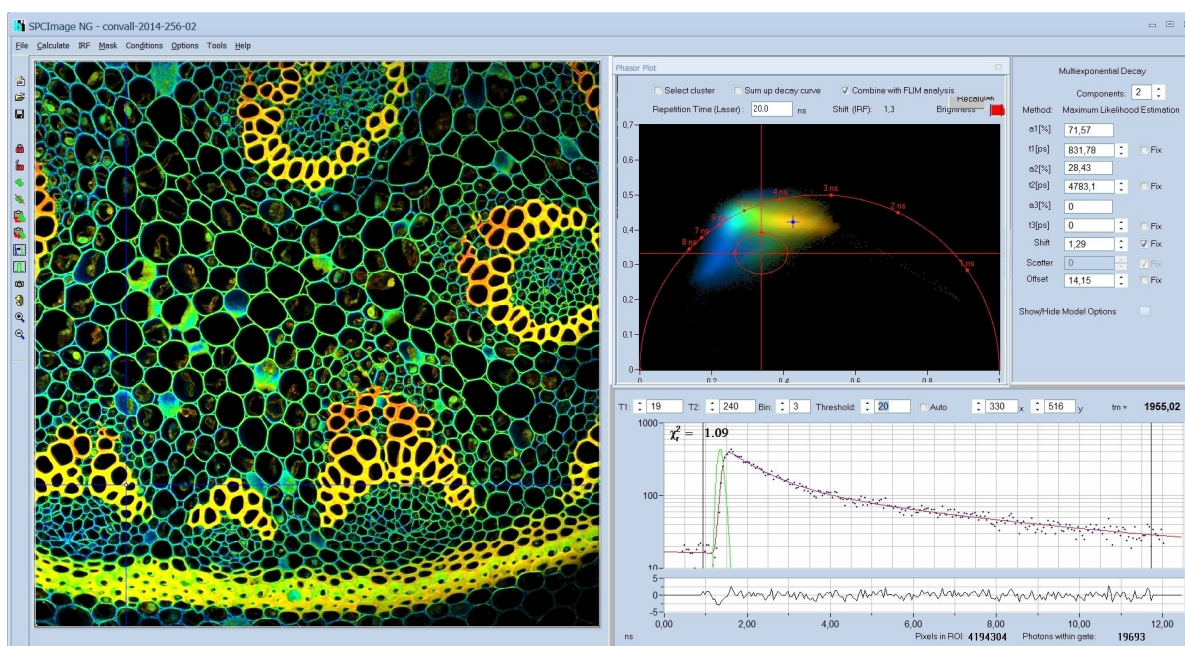


Fig. 48: Example of SPCImage NG main panel. Combination of time-domain analysis (left and lower right) and phasor plot (upper right)

### Deconvolution and Fit Procedure

SPCImage NG runs an iterative fit and de-convolution procedure on the decay data of the individual pixels of the FLIM images. In the simplest case, the result is the lifetime of the decay functions in the individual pixels. For complex decay functions the fit procedure delivers the lifetimes and amplitudes of the decay components. SPCImage then creates colour-coded images of the amplitude- or intensity-weighted lifetimes in the pixels, images of the lifetimes or amplitudes of the decay components, images of lifetime or amplitude ratios, and images of other combinations of decay parameters, such as FRET intensities, FRET distances, bound-unbound ratios, or the fluorescence-lifetime redox ratio, FLIRR. A few examples are shown in Fig. 49 and Fig. 50. For details please see [3, 31, 20].

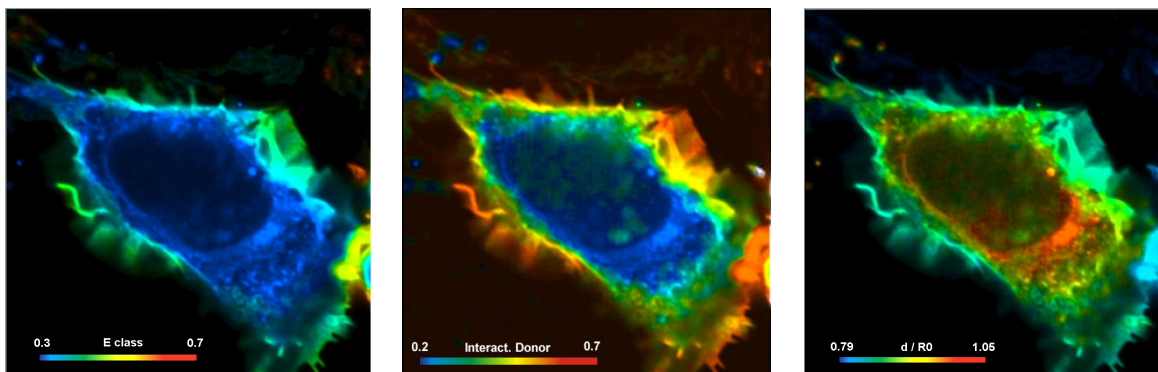


Fig. 49: Cell with interacting proteins, labelled with a FRET donor and a FRET acceptor. Left to right: Classic FRET efficiency, fraction of interacting donor, FRET distance

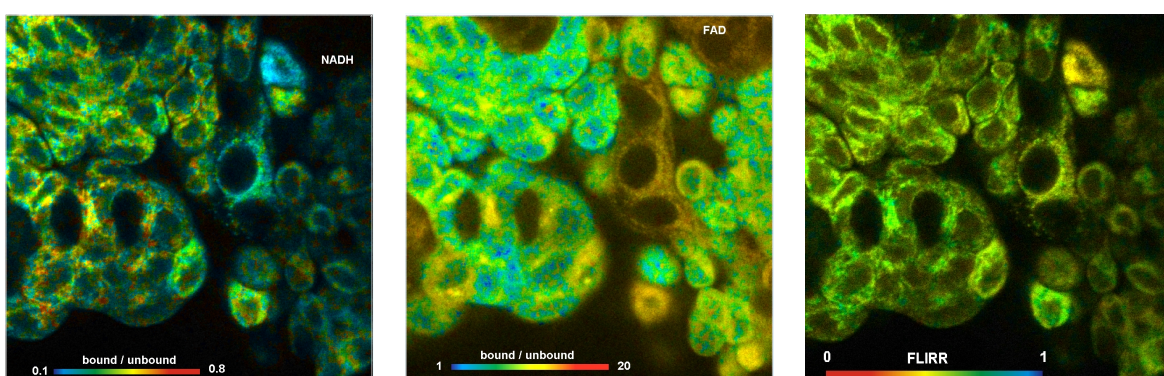


Fig. 50: Metabolic FLIM. Bound-unbound ratio of NADH, Bound/unbound ratio of FAD, Fluorescence-Lifetime Redox Ratio, FLIRR.

### ***GPU Processing***

SPCImage NG uses GPU (Graphics Processor Unit) processing. GPU processing is running on NVIDIA cards and a number of other NVIDIA-compatible devices. The TCSPC data are transferred into the GPU, which then runs the de-convolution and fit procedure for a large number of pixels in parallel. This way, data processing times for large images are reduced from formerly more than 10 minutes to a few seconds.

### ***Maximum-Likelihood Algorithm***

Unlike previous SPCImage versions, SPCImage NG uses a maximum-likelihood algorithm (or maximum-likelihood estimation, MLE) for fitting the data. In contrast to the usual least-square fit, the MLE algorithm takes into account the Poissonian distribution of the photon numbers. Compared to the least-square method, the fit accuracy is improved especially for low photon numbers, and there is no bias toward shorter lifetime as it is often observed for the least-square fit. For comparison with older data sets the weighted least-square fit and the first-moment algorithms of the previous SPCImage versions are still available in SPCImage NG.

### ***Instrument-Response Function***

SPCImage NG avoids troublesome recording of an instrument response function (IRF) for each FLIM measurement. This is achieved by modelling the IRF with a generic function. The parameters of this function are determined by fitting it to the FLIM data together with the selected decay model. The

results of this procedure are so good that an accurate IRF is obtained even for decay functions containing ultra-fast components, see Fig. 51. For details please see SPCImage chapter in [3, 31].

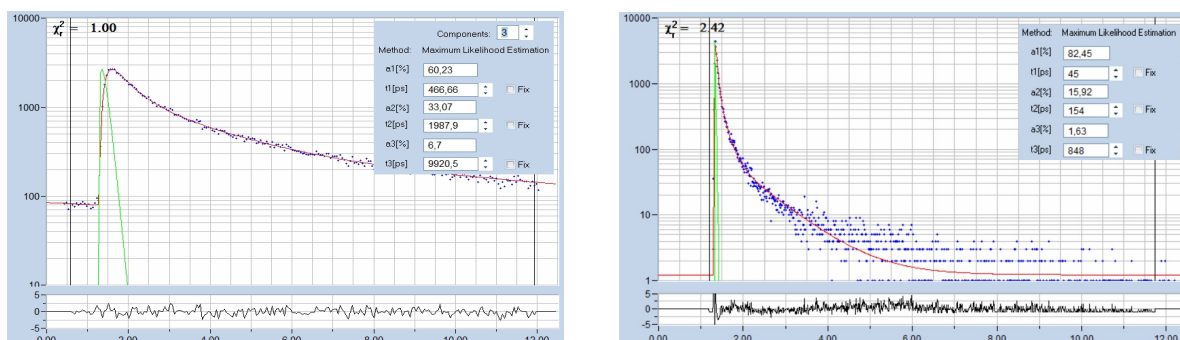


Fig. 51: Synthetic IRF. Left: Autofluorescence of cells, ps diode laser, HPM-100-40. Right: Sample with extremely fast decay component, femtosecond fibre laser, HPM-100-06

## Phasor Plot

SPCImage NG combines time-domain multi-exponential decay analysis with a phasor plot. In the phasor plot, the decay data in the individual pixels are expressed as phase and amplitude values in a polar diagram [43]. Independently of their location in the image, pixels with similar decay signature form clusters in the phasor plot. Different phasor clusters can be selected, and the corresponding pixels back-annotated in the time-domain FLIM images. The decay functions of the pixels within the selected phasor range can be combined into a single decay curve of high photon number. This curve can be analysed at high accuracy, revealing decay components that are not visible by normal pixel-by-pixel analysis [19]. An example is shown in Fig. 52.

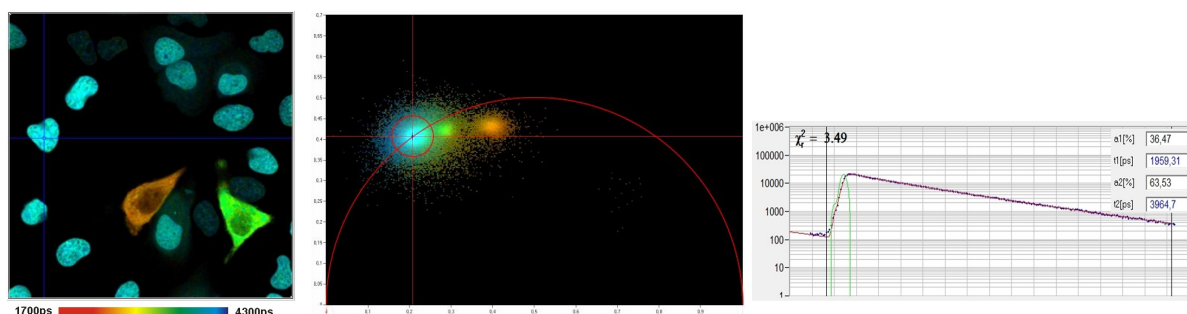


Fig. 52: Combination of time-domain analysis with phasor plot. Left to right: Lifetime image, phasor plot, decay curve of combined pixels within selected phasor range

## Image Segmentation

SPCImage NG therefore provides automatic image segmentation functions via the phasor plot and 2D histograms of the decay parameters. Areas with different decay signature form separate clusters in these presentations. Interesting clusters can be selected and back-annotated in the images. The decay data of the corresponding pixels are combined into a single decay curve with extremely high photon number. Multi-exponential decay analysis on the combined data delivers precision decay parameters even if the photon numbers in the individual pixels are low. An example is shown in Fig. 53.

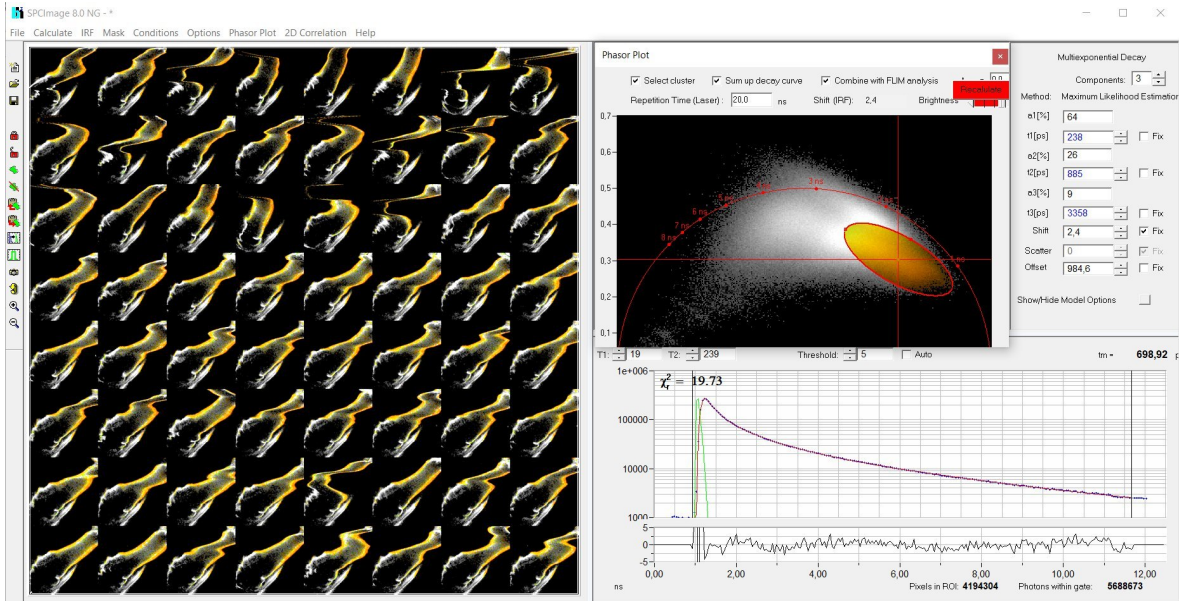


Fig. 53: Image segmentation on temporal-mosaic FLIM data of a live water flea

### Single-Curve Analysis

SPCImage can also be used to analyse single decay curves, The data can come from traditional cuvette experiments, or from the combined pixels of a FLIM recording. An example is shown in Fig. 54.

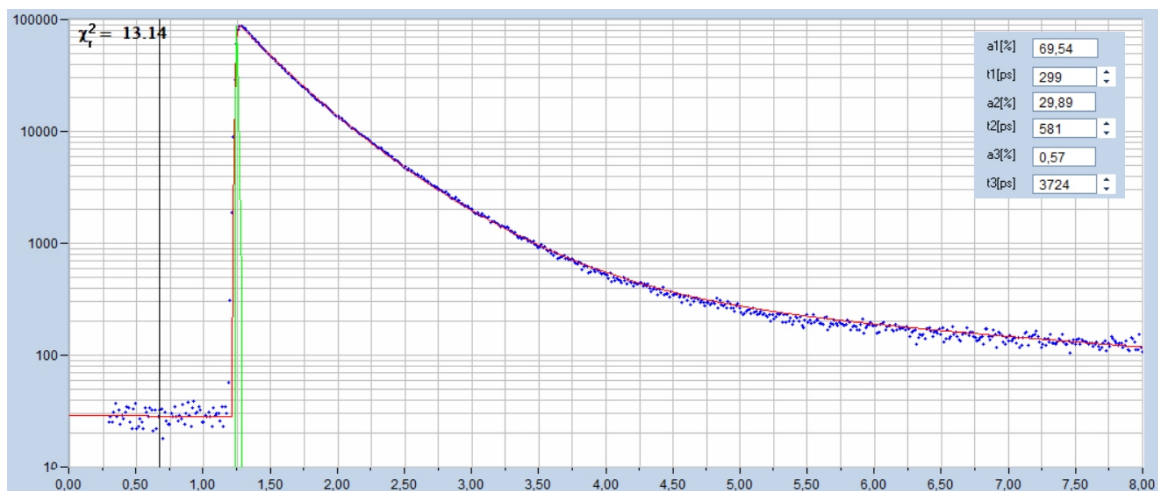


Fig. 54: SPCImage used for fluorescence decay analysis of single curves. NADH dissolved in water, recorded with bh DCS-120 MP FLIM system.

## Applications

### Molecular Imaging

FLIM uses the fluorescence decay function of a fluorophore as an indicator of its molecular environment. The fluorescence decay function, within reasonable limits, neither depends on the fluorophore concentration nor on the excitation power, or other instrumental details. This is a striking advantage over intensity-based imaging techniques. If fluorescence in a sample is excited (Fig. 55, left) the emission intensity (second left) depends not only on possible interaction of the fluorophore with the molecular environment but also on the fluorophore concentration, on possible absorption in the sample, on the excitation power, and on the light collection efficiency of the optics. Changes in the molecular environment can thus not be distinguished from changes in these parameters. Spectral measurements (second right) are able to distinguish between different fluorophores. However, changes in the local environment usually do not cause changes in the shape of the spectrum. The fluorescence lifetime of a fluorophore however (Fig. 55, right), only depends on the interaction of the fluorophore with the molecular environment.

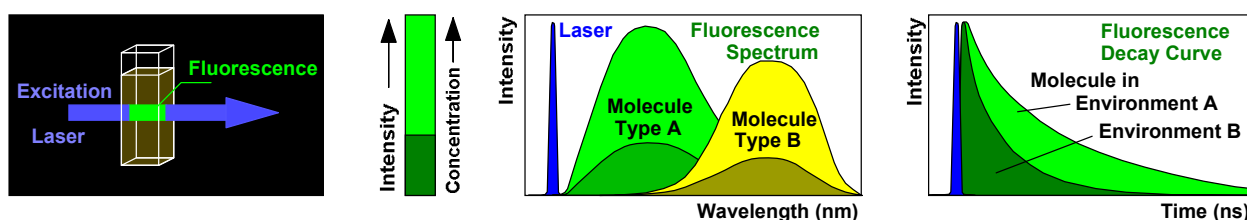


Fig. 55: Fluorescence. Left to right: Excitation light is absorbed by a fluorophore, and fluorescence is emitted at a longer wavelength. The fluorescence intensity varies with concentration. The fluorescence spectrum is characteristic of the type of the fluorophore. The fluorescence decay function is an indicator of interaction of the fluorophore with its molecular environment.

By using the fluorescence lifetime, or, more precisely, the shape of the fluorescence decay function, molecular effects can therefore be investigated independently of the unknown and usually variable fluorophore concentration [31, 37, 64]. Common FLIM applications are ion concentration measurements, probing of protein interaction via FRET, and the probing of the metabolic state and the cell viability via the fluorescence decay parameters of NADH and FAD. FLIM may also find application in plant physiology because the fluorescence lifetime of chlorophyll changes with the photosynthesis activity.

### Förster Resonance Energy Transfer: FRET

A particularly efficient molecular interaction is Förster resonance energy transfer, or FRET. The effect was found by Theodor Förster in 1946 [53]. FRET is a dipole-dipole interaction of two molecules in which the emission band of one molecule overlaps the absorption band of the other. In this case the energy from the first molecule, the donor, transfers into the second one, the acceptor, see Fig. 56, left. FRET results in an extremely efficient quenching of the donor fluorescence and, consequently, in a considerable decrease of the donor lifetime, see Fig. 56, right.

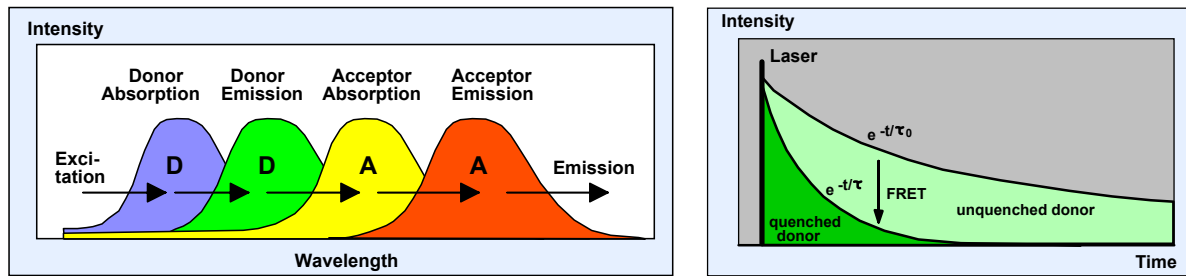


Fig. 56: Fluorescence Resonance Energy Transfer (FRET)

The energy transfer rate from the donor to the acceptor increase with the sixth power of the reciprocal distance. Therefore it is noticeable only at distances shorter than 10 nm [64]. FRET is therefore used as a tool to investigate protein-protein interaction. Different proteins are labelled with the donor and the acceptor, and FRET is used as an indicator of the binding between these proteins. Steady-state FRET measurements have the problem that the relative concentration of donor and acceptor varies, that the donor emission spectrally extends into the acceptor emission, and that a fraction of the acceptor is excited directly. FLIM does not have these problems because all it needs is to record a lifetime image at the donor emission wavelength. There are hundreds of publications using FLIM FRET, please see [31] for references.

Fig. 57 shows FRET in a cultured live HEK cell. The cell is expressing two proteins, one labelled with CFP, the other with YFP. FRET occurs in the places where the proteins interact. The associated changes in the donor lifetime are clearly visible in the lifetime image shown in Fig. 57, left.

FLIM is not only able to detect FRET without interference by donor and acceptor bleedthrough, it even delivers independent images of the donor-acceptor distance and the fraction of interacting donor. Such images can be obtained by double-exponential analysis of the FLIM data: The interacting donor fraction delivers a fast, the non-interacting fraction a slow decay component. The ratio of the two lifetimes is directly related to the donor-acceptor distance, the ratio of the amplitudes of the components is the ratio of interacting and non-interacting donor. Images which resolve these two parameters of the FRET system are shown in Fig. 57, middle and right.

Remarkably, double exponential FRET does not need an external lifetime reference: The reference lifetime is the slow decay component, originating from the non-interaction donor. Please see [3, 25, 31] for details and for further references.

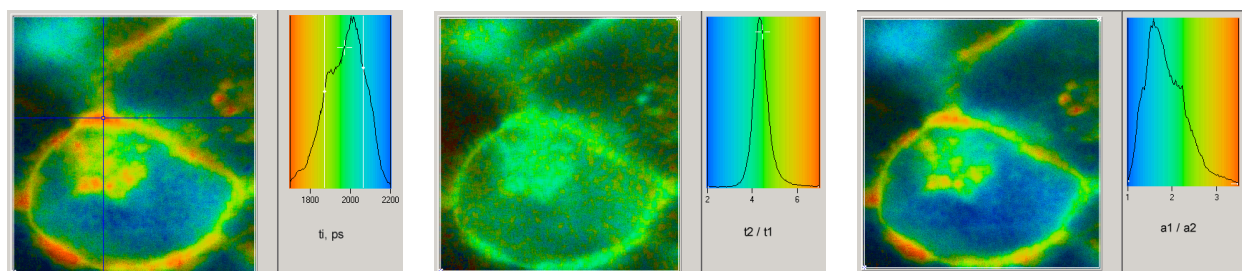


Fig. 57: FRET in HEK cell expressing proteins labelled with CFP and YFP. Left: Lifetime image at donor wavelength, showing lifetime changes by FRET. Middle and right: FRET results obtained by double-exponential lifetime analysis. Ratio of the lifetimes of the decay components,  $t2/t1 = \tau_0/\tau_{\text{fret}}$ , and ratio of the interacting and non-interacting donor fractions,  $a1/a2 = N_{\text{fret}}/N_0$ .

### Autofluorescence

Biological tissue contains a wide variety of endogenous fluorophores [69]. Fluorescence lifetime imaging improves the contrast of separation of the different fluorophores. Moreover, TCSPC FLIM is more and more introduced into clinical applications. In these applications ‘label-free’ imaging is needed because staining the tissue with exogenous fluorophores is either not possible or not permitted. FLIM delivers a wealth of additional image information which often makes the use of exogenous fluorophores unnecessary [42, 60, 70, 73, 72, 76].

The most important capability of autofluorescence FLIM is, however, that it delivers information on the metabolic state of the cells or the tissue under investigation. The most promising signals come from NAD(P)H (nicotinamide adenine (pyridine) dinucleotide) and FAD (flavin adenine dinucleotide). NAD(P)H and FAD are coenzymes involved in the cell metabolism. NAD(P)H and FAD are unique in the sense that their fluorescence intensities and fluorescence decay functions bears direct information on the metabolic state of the cells.

The fluorescence lifetimes of NAD(P)H and FAD depend on the binding to proteins [63, 64, 68]. Unbound NAD(P)H has a fluorescence lifetime of about 0.3 to 0.5 ns. When NAD(P)H binds to proteins the lifetime typically increases to a few ns [64]. For FAD the effect of binding is opposite: Bound FAD has a lifetime of a few 100 ps, unbound FAD of a few ns. The resulting decay functions are thus double exponential. Typical decay functions of NAD(P)H and FAD in cells are shown in Fig. 58.

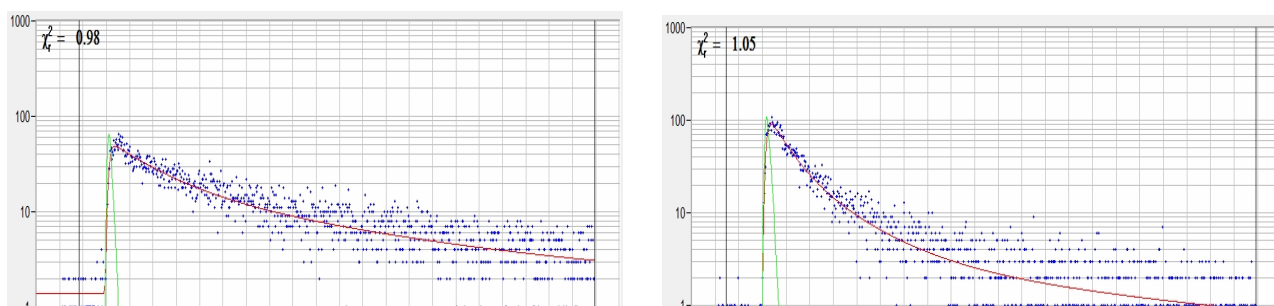


Fig. 58: Typical decay functions of NAD(P)H (left) and FAD (right). The blue dots are the data points, the red curve is a fit with a double-exponential decay model. Recorded from human epithelium cells by bh metabolic FLIM system [3].

The ratio of the amplitudes of the decay components,  $a_1/a_2$ , often called ‘amplitude ratio’, directly represents the concentration ratio of unbound/bound NADH or bound/unbound FAD, see Fig. 59. The ratios of bound to unbound NAD(P)H and unbound to bound FAD depends on the type of the metabolism. A cell can run both a oxidative metabolism (oxidative phosphorylation) and a reductive one (glycolysis). A shift from oxidative phosphorylation to glycolysis is accompanied by a decrease of the bound fractions of NAD(P)H and FAD. The resulting change in the  $a_1/a_2$  ratio is shown schematically in Fig. 59, compare upper row and lower row.

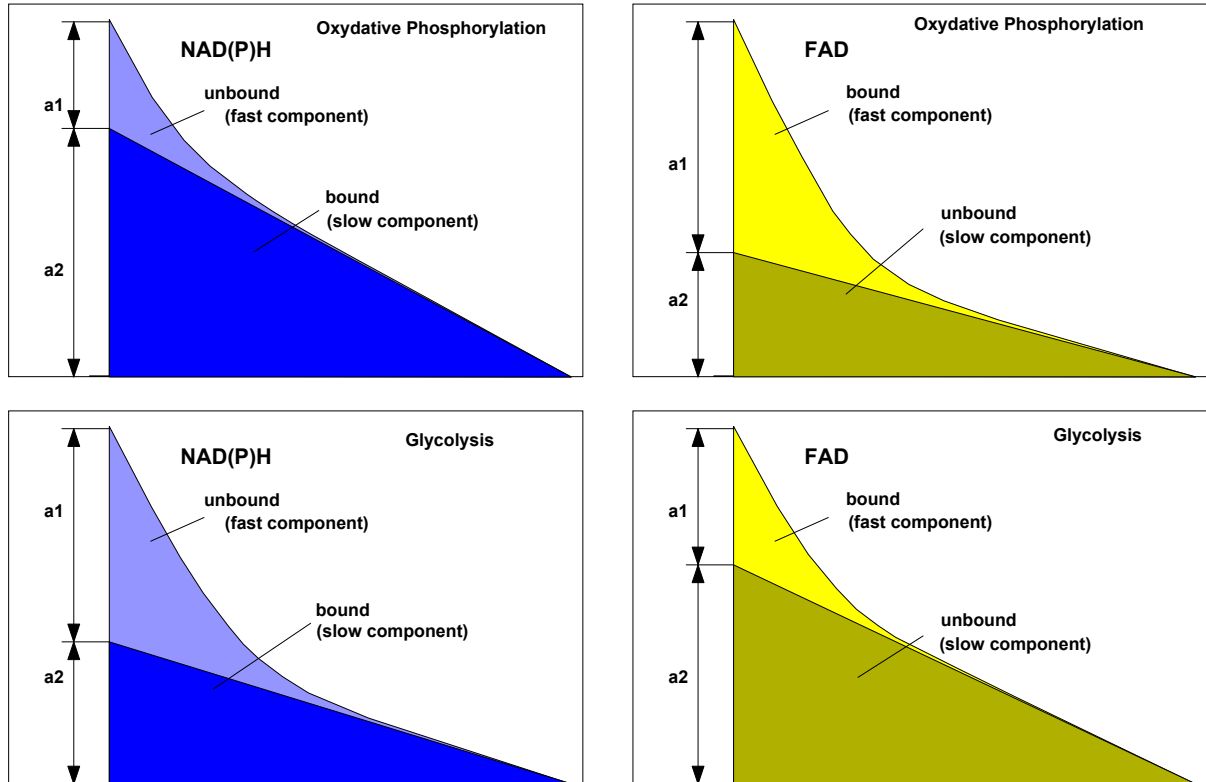


Fig. 59: The composition of the decay functions of NAD(P)H and FAD and changes with the metabolic state. Effect of metabolic state on the decay curves exaggerated.

The effects shown in Fig. 59, left are seen in many NAD(P)H FLIM recordings. A few examples are shown in Fig. 60. The figure shows FLIM images of the amplitude-weighted lifetimes,  $t_m$ , (upper row) and amplitudes of the fast decay component,  $a_1$ , of various cells. The left three cells are tumor cells, the right two are normal ones. In agreement with Fig. 59, there is a clear trend in the  $t_m$  and the  $a_1$  from the tumor cells to the normal ones.

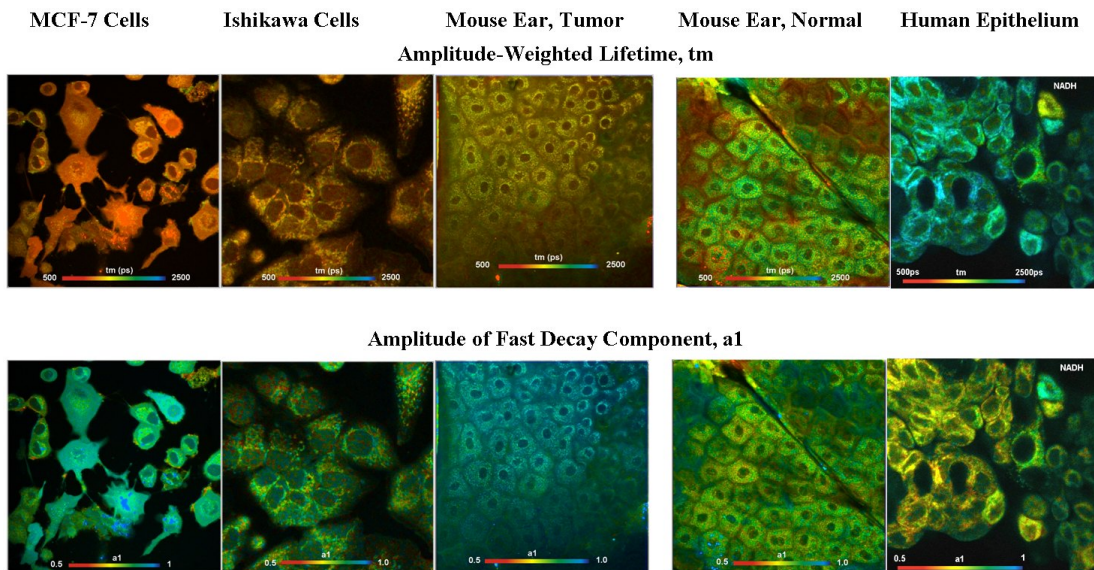


Fig. 60: Images of amplitude-weighted lifetimes,  $t_m$ , (upper row) and amplitudes,  $a_1$ , of various cells. The left three cells are tumor cells, the right two are normal.

FAD FLIM images comparing tumor cells and normal cells are still relatively rare. As shown in Fig. 59, the change in the lifetime and in the amplitudes for the FAD should go into the opposite direction as for the NAD(P)H. Although there is still some controversy about the direction of the effect, the opposite lifetime change is confirmed by results of the group of Melissa Skala at Vanderbilt University [77] see Fig. 61.

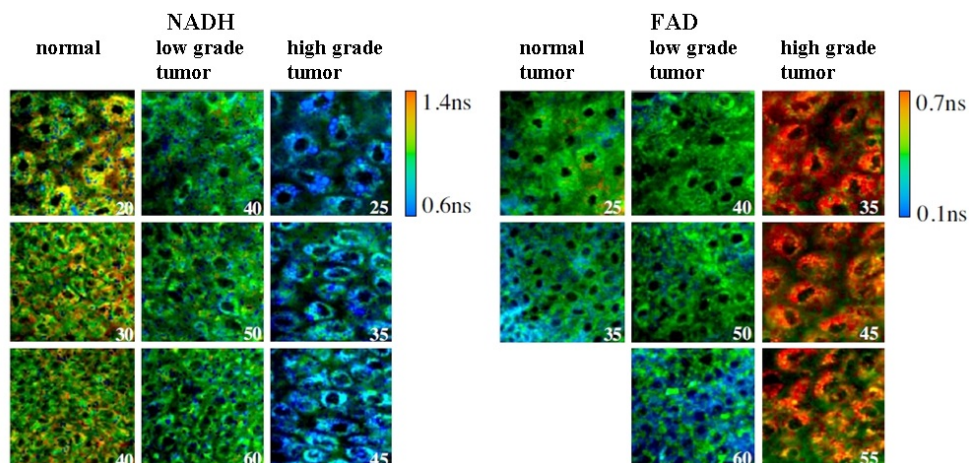


Fig. 61: Change in the mean (amplitude-weighted) lifetime of NADH and FAD with the state of the cells, from normal (oxidative phosphorylation) to high-grade tumor (glycolysis). With permission, from [77].

The opposite changes in the decay curves of NAD(P)H and FAD are a possible explanation of numerous discrepancies in fluorescence lifetimes measured in tumours. There have been as many reports for decreased lifetime as for increased ones. The source of the discrepancies is probably that the measurements did not cleanly separate the signals from NADH and FAD. This can easily happen because both the excitation and the emission spectra are strongly overlapping. Depending on which fluorophore dominates the net decay function the result can indeed be a decrease or an increase of the lifetime in the tumor compared to normal tissue. The problem can be solved by using the correct excitation and emission wavelengths. The DCS system provides laser multiplexing functions to perform the recordings quasi-simultaneously, thus avoiding errors by photobleaching or metabolism-induced dynamic effects during the measurement. For examples see [3, 31]. There is an increasing number of papers about NADH / FAD FLIM [38, 39, 51, 64, 65, 66, 73, 77, 78, 81, 83]. Please see [3] or [31] for more references and for a detailed discussion of the technique.

### ***Oxygen Sensing by PLIM***

Oxygen sensing is based on the quenching of the phosphorescence decay of (endogenous) phosphorescent dyes by oxygen. Two examples are shown in Fig. 62. The figure shows PLIM images of cultured human embryonic kidney cells incubated with a palladium-based phosphorescence dye. Fig. 62, left was recorded under atmospheric oxygen partial pressure. The maximum of the lifetime distribution over the pixels (upper right) is at 75  $\mu\text{s}$ . Fig. 62, right, was recorded under decreased oxygen partial pressure. As can be seen, the maximum of the lifetime distribution has shifted to 144  $\mu\text{s}$ .

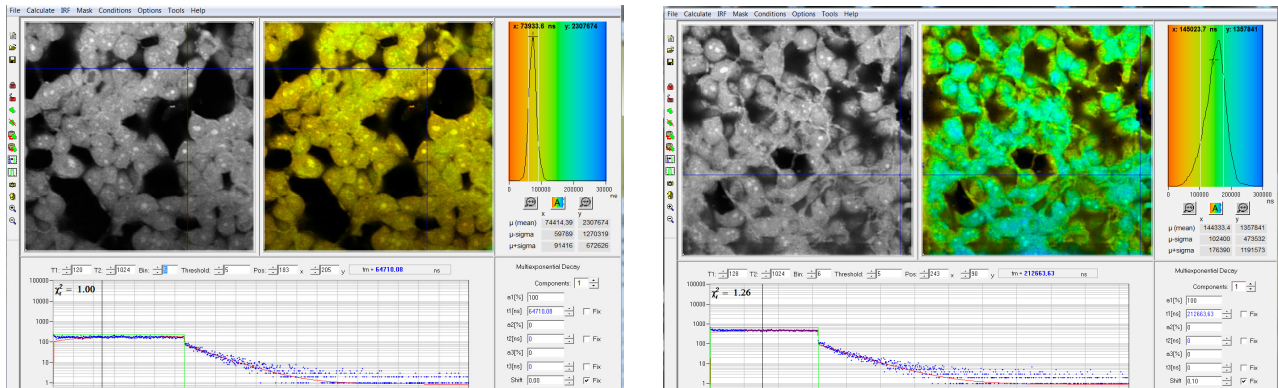


Fig. 62: HEK cells incubated with a palladium dye imaged under different oxygen partial pressure. Left: Atmospheric O<sub>2</sub> pressure. Right: reduced oxygen partial pressure. Recorded by bh DCS-120 confocal scanning system, data analysis by bh SPCImage. Lifetime scale 0 (red) to 300  $\mu$ s (blue). Phosphorescence lifetime at the Cursor-Position 65  $\mu$ s. The maximum of the lifetime distribution over the pixels is at 75  $\mu$ s.

### Simultaneous Recording of Oxygen and NAD(P)H Images

The DCS-120 system is able to record phosphorescence and fluorescence lifetime images simultaneously [3]. The function can be used to obtain metabolic information from the NAD(P)H and compare the results with the oxygen concentration in the cells [57, 62, 74]. Simultaneously recorded fluorescence and phosphorescence lifetime images of live cultured human embryonic kidney cells stained with 5,10,15,20-tetrakis(4-carboxyphenyl)porphyrin-Pd(II) are shown in Fig. 63. The FLIM and PLIM images on the left were recorded under atmospheric oxygen concentration. The images on the right were recorded after adding sodium sulphite ( $\text{Na}_2\text{SO}_3$ ).  $\text{Na}_2\text{SO}_3$  binds oxygen. The oxygen concentration is therefore low. It can clearly be seen that the phosphorescence lifetime became longer, indicating there is indeed less oxygen (please note different colour scales). In the FLIM image, it can be seen that the amplitude-weighted lifetime,  $\tau_m$ , of the NADH has decreased.

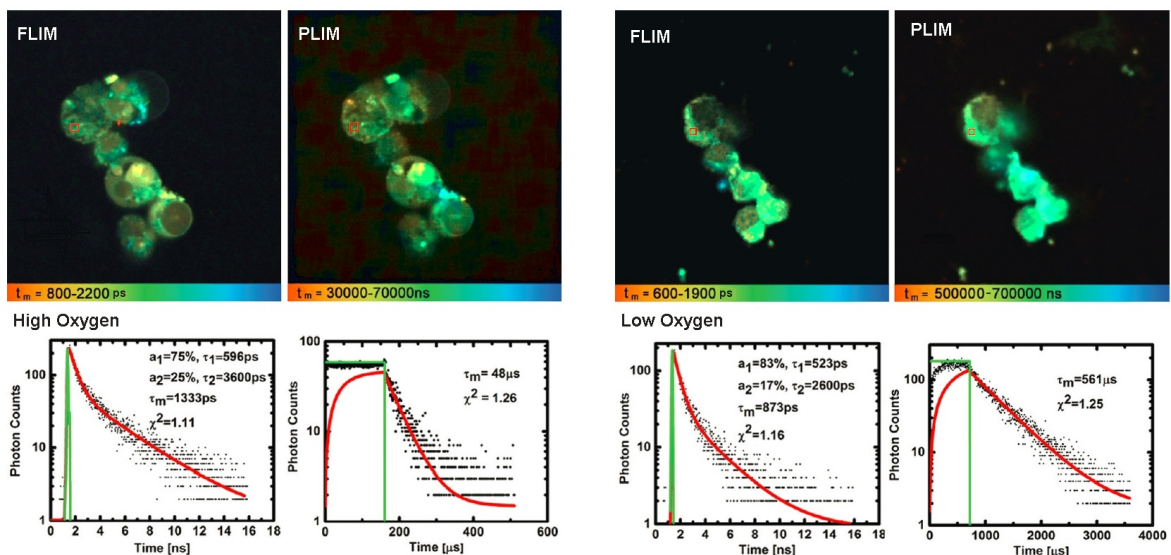


Fig. 63: Simultaneous FLIM/PLIM of human embryonic kidney cells. Left: High (atmospheric oxygen concentration). Right: Low oxygen concentration. Upper row FLIM and PLIM images, lower row decay curves in indicated position. Lifetime-colour scale given underneath the images. bh DCS-120 confocal scanning FLIM system, excitation wavelength 375 nm. Adapted from Shcheslavskiy et al. [74].

### Plant Physiology

Two examples of FLIM of plant tissue are shown in Fig. 64 and Fig. 65. The fluorescence is dominated by the fluorescence of chlorophyll and the fluorescence of flavines. Multi-wavelength FLIM images of a moss leaf recorded with the bh multi-spectral FLIM detector are shown in Fig. 64.

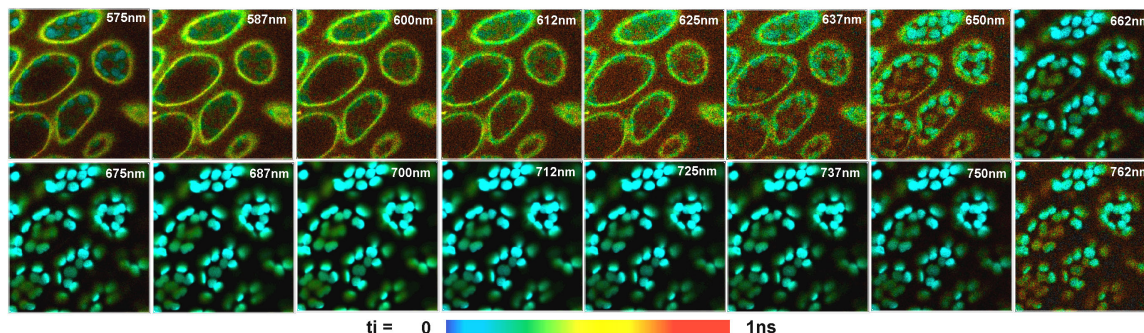


Fig. 64: Multi-spectral FLIM of plant tissue. Moss leaf, excitation at 405 nm, wavelength from 575 nm to 762 nm. DCS-120, MW FLIM detector. Image size 256x256 pixels, 64 time channels, 16 wavelength channels.

The fluorescence of chlorophyll competes with the energy transfer into the photosynthesis channels. Thus, the fluorescence lifetime and its change on illumination is a sensitive indicator of the photosynthesis efficiency. The change in the fluorescence lifetime of the chloroplasts in a moss leaf on exposure to light can be recorded by time-series FLIM, see Fig. 65.

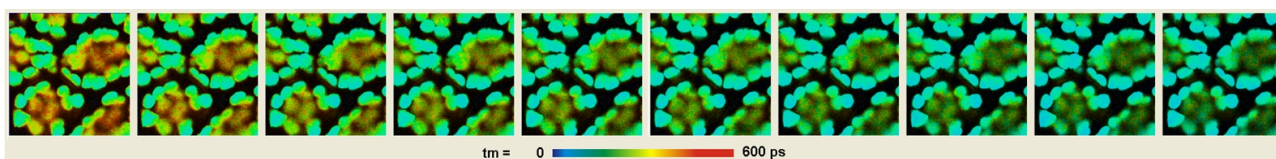


Fig. 65: Change of the fluorescence lifetime of chlorophyll with time of exposure. Moss leaf, excitation at 445 nm, 256x256 pixels, 1 image per second.

Faster effects down to the millisecond time scale can be recorded by temporal mosaic FLIM or FLITS, [31, 32] see Fig. 40 and Fig. 41 of this brochure.

### Summary

The DCS-120 system records lifetime images at high spatial and temporal resolution, extremely high sensitivity, and short acquisition time. Recently introduced 64-bit SPCM operating software has increased the image format of FLIM into the megapixel region. Single-, dual-, multi-wavelength FLIM is now recorded at unprecedented image quality. Moreover, the large memory space available in the 64 bit environment made it possible to implement advanced FLIM techniques, like time series recording and Z stack recording by Mosaic recording. Physiological effects down to the millisecond range can be resolved by triggered mosaic FLIM and by FLITS. Metabolic effects can be recorded by FLIM and correlated with changes in the oxygen concentration simultaneously measured by PLIM. No other FLIM technique and no other FLIM system offers a similar range of advanced capabilities.

## Specifications

### Scan head

Optical principle	confocal, beam scanning by fast galvanometer mirrors
Laser inputs	two independent inputs, fibre coupled or free beam
Laser power regulation, optical	continuously variable via neutral-density filter wheels
Outputs to detectors	two outputs, detectors are directly attached
Main beamsplitter versions	multi-band dichroic, wideband, multiphoton
Secondary beamsplitter wheel	3 dichroic beamsplitters, polarising beamsplitter, 100% to channel1, 100% to channel2
Pinholes	independent pinhole wheel for each channel
Pinhole size	11 pinholes, from about 0.5 to 10 AU
Emission filters	2 filter sliders per channel
Connection to microscope	adapter to left side port or port on top of microscope
Coupling of lasers into scan head (visible)	single-mode fibres, Point-Source type, separate for each laser
Coupling of laser into scan head (Ti:Sa)	free beam, 1 to 2 mm diameter

### Scan Controller

Principle	Digital waveform generation, scan waveforms generated by hardware
Scan waveform	linear ramp with cycloid flyback
Scan format	line, frame, or single point
Frame size, frame scan	16x16 to 4096x4096 pixels
line scan	16 to 4096 pixels
X scan	continuous or pixel-by-pixel
Y scan	line by line
Laser power control, electrical	via electrical signal to lasers
Laser multiplexing	frame by frame, line by line, or within one pixel
Beam blanking	during flyback and when scan is stopped
Scan rate	automatic selection of fastest rate or manual selection
minimum pixel time for frame size	64x64 128x128 256x256 512x512 1024x1024 2048x2048
Zoom=1	25.6µs 12.8µs 6.4µs 3.2µs 1.6µs 1.2µs
Zoom=8	6.4µs 3.2µs 1.6µs 0.8µs 0.6µs 0.5µs
minimum frame time for frame size	64x64 128x128 256x256 512x512 1024x1024 2048x2048
Zoom=1	0.19s 0.37s 0.64s 1.24s 2.6s 6.5s
Zoom=8	0.037s 0.074s 0.173s 0.320s 1.0s 2.7s
Scan area definition	via zoom and offset or interactive via cursors during preview
Fast preview function	1 second per frame, 128 x 128 pixels
Beam park function	via cursor in preview image or cursor in FLIM image
Laser control	2 Lasers, on/off, frame, line, pxl multiplexing

### Diode lasers

Number of lasers simultaneously operated	bh BDL-SMC or BDL-SMN laser 2
Wavelengths	375nm, 405nm, 445nm, 473nm, 488nm, 510nm, 640nm, 685nm, 785nm
Pulse width, typical	30 to 70 ps
Pulse frequency	20MHz, 50MHz, 80MHz, CW
Power in picosecond mode	0.25mW to 1mW injected into fibre. Depends on wavelength version.
Power in CW mode	10 to 40mW injected into fibre. Depends on wavelength version.

### Other lasers

Visible and UV range	any ps pulsed laser of 20 to 80 MHz repetition rate
Coupling requirements	Point-Source Kineflex compatible fibre adapter
Wavelength	any wavelength from 400nm to 800nm
fs NIR Lasers for multiphoton operation	any fs laser
Coupling requirements	free beam, diameter 1 to 2 mm
Wavelength	700 to 1200 nm

### Detectors (standard)

Spectral Range	bh HPM-100-40 hybrid detector 300 to 710nm
Peak quantum efficiency	40 to 50%
IRF width with bh diode laser	120 to 130 ps
Active area	3mm
Background count rate, thermal	300 to 2000 counts per second
Power supply, gain control, overload shutdown	via DCC-100 controller of TCSPC system

### Detectors (optional)

Spectral Range	bh HPM-100-06 and HPM-100-07 hybrid detectors 290 nm to 600 nm      220 to 850 nm
----------------	--



## DCS-120 FLIM System

Peak quantum efficiency	20 % (at 400nm)	26% at 290 nm, 22% at 400nm
System IRF width with fs Ti:Sa laser	<20 ps	
System IRF width with bh ps diode laser	38 to 90 ps	
Active area	3mm	
Background count rate, thermal	100 to 1000 counts per second	
Power supply, gain control, overload shutdown	via DCC-100 controller of TCSPC system	

### Detectors (optional)

	<b>bh HPM-100-50 hybrid detector</b>	
Spectral Range	400 to 900nm	
Peak quantum efficiency	12 to 15%	
IRF width with bh diode laser	150 to 200 ps	
Active area	3mm	
Background count rate, thermal	1000 to 8000 counts per second	
Power supply, gain control, overload shutdown	via DCC-100 controller of TCSPC system	

### Detectors (optional)

	<b>bh MW FLIM GaAsP Multi-Wavelength FLIM detector</b>	
Spectral range	380 to 700nm	
Number of wavelength channels	16	
Spectral width of wavelength channels	12.5 nm	
IRF width with bh diode laser	200 to 250 ps	
Power supply and overload shutdown	via DCC-100 controller of TCSPC system	

### TCSPC System

	<b>bh SPC-150, SPC-150N, or SPC-160 modules, see [31] for details</b>		
Number of parallel modules (recording channels)	2		
Number of detector (routing) channels in each module	16 (for multi-spectral FLIM detector)		
Principle	Advanced TAC/ADC principle [31]		
Electrical time resolution	2.3 ps rms		
Minimum time channel width	813 fs		
Dead time	100 ns		
Saturated count rate	10 MHz per channel		
Dual-time-base operation	via micro times from TAC and via macro time clock		
Source of macro time clock	internal 40MHz clock or from laser		
Input from detector	constant-fraction discriminator		
Reference (SYNC) input	constant-fraction discriminator		
Synchronisation with scanning	via frame clock, line clock and pixel clock pulses		
Scan rate	any scan rate		
Synchronisation with laser multiplexing	via routing function		
Recording of multi-wavelength data	simultaneous, via routing function		
Basic acquisition principles	on-board-buildup of photon distributions buildup of photon distributions in computer memory generation of parameter-tagged single-photon data online auto or cross correlation and PCH		
Operation modes	f(t), oscilloscope, f(txy), f(t,T), f(t) continuous flow FIFO (correlation / FCS / MCS) mode Scan Sync In imaging, Scan Sync In with continuous flow FIFO imaging, with MCS imaging, mosaic imaging, time-series imaging Multi-detector operation, laser multiplexing operation cycle and repeat function, autosave function		
Max. Image size, pixels (SPCM 64 bit software)	2048x2048	1024x1024	512x512
No of time channels, see [31]	256	1024	4096

### Data Acquisition Software, please see [31] for details

Operating system	Windows 7 or Windows 10, 64 bit		
Loading of system configuration	single click in predefined setup panel		
Start / stop of measurement	by operator or by timer, starts with start of scan, stops with end of frame		
Online calculation and display, FLIM, PLIM	in intervals of Display Time, min. 1 second		
Online calculation and display, FCS, PCH	in intervals of Display Time, min. 1 second		
Number of images displayed simultaneously	max 8		
Number of curves (Decay, FCS, PCH, Multiscaler)	16 in one curve window		
Cycle, repeat, autosave functions	user-defined, used for for time-series recording, Z stack FLIM, microscope-controlled time series		
Saving of measurement data	User command or autosave function		
Link to SPCImage data analysis	Optional saving of parameter-tagged single-photon data automatically after end of measurement or by user command		

## References

1. E. Baggaley, S. W. Botchway, J. W. Haycock, H. Morris, I. V. Sazanovich, J. A. G. Williams, J. A. Weinstein, Long-lived metal complexes open up microsecond lifetime imaging microscopy under multiphoton excitation: from FLIM to PLIM and beyond. *Chem. Sci.* 5, 879-886 (2014)
2. E. Baggaley, M. R. Gill, N. H. Green, D. Turton, I. V. Sazanovich, S. W. Botchway, C. Smythe, J. W. Haycock, J. A. Weinstein, J. A. Thomas, Dinuclear Ruthenium(II) Complexes as Two-Photon, Time-Resolved Emission Microscopy Probes for Cellular DNA. *Angew. Chem. Int. Ed. Engl.* 53, 3367-3371 (2014)
3. Becker & Hickl GmbH, DCS-120 Confocal and Multiphoton FLIM Systems, user handbook, 9th edition 2021. [www.becker-hickl.com](http://www.becker-hickl.com), printed copies available
4. Becker & Hickl GmbH, The HPM-100-40 hybrid detector. Application note, available on [www.becker-hickl.com](http://www.becker-hickl.com)
5. Becker & Hickl GmbH, Spatially resolved recording of fluorescence-lifetime transients by line-scanning TCSPC. Application note, available on [www.becker-hickl.com](http://www.becker-hickl.com)
6. Becker & Hickl GmbH, DCS-120 Confocal Scanning FLIM System: Two-Photon Excitation with Non-Descanned Detection. Application note, available on [www.becker-hickl.com](http://www.becker-hickl.com)
7. Becker & Hickl GmbH, DCS-120 Confocal FLIM system with wideband beamsplitter. Application note, available on [www.becker-hickl.com](http://www.becker-hickl.com)
8. Becker & Hickl GmbH, Non-Descanned FLIM Detection in Multiphoton Microscopes. Application note, available on [www.becker-hickl.com](http://www.becker-hickl.com)
9. Becker & Hickl GmbH, DCS-120 Confocal Scanning FLIM System with User-Specific Lasers: FIANIUM SC400 Laser. Application note, available on [www.becker-hickl.com](http://www.becker-hickl.com)
10. Becker & Hickl GmbH, DCS-120 Confocal Scanning FLIM System with User-Specific Lasers: NKT SuperK EXTREME Laser. Application note, available on [www.becker-hickl.com](http://www.becker-hickl.com)
11. Becker & Hickl GmbH, Megapixel FLIM with bh TCSPC Modules - The New SPCM 64-bit Software. Application note, available on [www.becker-hickl.com](http://www.becker-hickl.com)
12. TCSPC at Wavelengths from 900 nm to 1700 nm. Application note, available on [www.becker-hickl.com](http://www.becker-hickl.com)
13. Becker & Hickl GmbH, Simultaneous Phosphorescence and Fluorescence Lifetime Imaging by Multi-Dimensional TCSPC and Multi-Pulse Excitation. Application note, available on [www.becker-hickl.com](http://www.becker-hickl.com)
14. Becker & Hickl GmbH, SPCM software runs online-FLIM at 10 images per second. Application note, available on [www.becker-hickl.com](http://www.becker-hickl.com)
15. Becker & Hickl GmbH, Sub-20ps IRF Width from Hybrid Detectors and MCP-PMTs. Application note, available on [www.becker-hickl.com](http://www.becker-hickl.com)
16. Becker & Hickl GmbH, Ultra-fast HPM Detectors Improve NAD(P)H FLIM. Application note, available on [www.becker-hickl.com](http://www.becker-hickl.com)
17. Becker & Hickl GmbH, Fast-Acquisition TCSPC FLIM System with sub-25 ps IRF width. Application note, available from [www.becker-hickl.com](http://www.becker-hickl.com)
18. Becker & Hickl GmbH, Fast-Acquisition TCSPC FLIM: What are the Options? Application note, available from [www.becker-hickl.com](http://www.becker-hickl.com)
19. Becker & Hickl GmbH, New SPCImage Version Combines Time-Domain Analysis with Phasor Plot. Application note, available on [www.becker-hickl.com](http://www.becker-hickl.com)
20. Becker & Hickl GmbH, SPCImage next generation FLIM data analysis software. Overview brochure, available on [www.becker-hickl.com](http://www.becker-hickl.com)
21. Becker & Hickl GmbH, Two-Photon FLIM with a Femtosecond Fibre Laser. Application note, available on [www.becker-hickl.com](http://www.becker-hickl.com)
22. Becker & Hickl GmbH, Modular FLIM systems for Zeiss LSM 510 and LSM 710 family laser scanning microscopes. User handbook. Available on [www.becker-hickl.com](http://www.becker-hickl.com)
23. W. Becker, A. Bergmann, C. Biskup, T. Zimmer, N. Klöcker, K. Benndorf, Multi-wavelength TCSPC lifetime imaging, *Proc. SPIE* 4620 79-84 (2002)
24. W. Becker, A. Bergmann, M.A. Hink, K. König, K. Benndorf, C. Biskup, Fluorescence lifetime imaging by time-correlated single photon counting, *Micr. Res. Techn.* 63, 58-66 (2004)
25. W. Becker, *Advanced time-correlated single-photon counting techniques*. Springer, Berlin, Heidelberg, New York, 2005
26. W. Becker, A. Bergmann, C. Biskup, Multi-Spectral Fluorescence Lifetime Imaging by TCSPC. *Micr. Res. Tech.* 70, 403-409 (2007)
27. W. Becker, B. Su, K. Weisshart, O. Holub, FLIM and FCS Detection in Laser-Scanning Microscopes: Increased Efficiency by GaAsP Hybrid Detectors. *Micr. Res. Tech.* 74, 804-811 (2011)
28. W. Becker, B. Su, A. Bergmann, K. Weisshart, O. Holub, Simultaneous Fluorescence and Phosphorescence Lifetime Imaging. *Proc. SPIE* 7903, 790320 (2011)
29. W. Becker, *Fluorescence Lifetime Imaging - Techniques and Applications*. *J. Microsc.* 247 (2) (2012)

30. W. Becker, V. Shcheslavskiy, FLIM with near-infrared dyes. *Proc. SPIE* 8588 (2013)
31. W. Becker, *The bh TCSPC handbook*. 9th edition. Becker & Hickl GmbH (2021), [www.becker-hickl.com](http://www.becker-hickl.com), printed copies available from bh
32. W. Becker, V. Shcheslavskiy, S. Frere, I. Slutsky, Spatially Resolved Recording of Transient Fluorescence-Lifetime Effects by Line-Scanning TCSPC. *Microsc. Res. Techn.* 77, 216-224 (2014)
33. W. Becker, *Introduction to Multi-Dimensional TCSPC*. In W. Becker (ed.) *Advanced time-correlated single photon counting applications*. Springer, Berlin, Heidelberg, New York (2015)
34. W. Becker, V. Shcheslavskiy, H. Studier, *TCSPC FLIM with Different Optical Scanning Techniques*, in W. Becker (ed.) *Advanced time-correlated single photon counting applications*. Springer, Berlin, Heidelberg, New York (2015)
35. W. Becker, A. Bergmann, L. Braun, *Metabolic Imaging with the DCS-120 Confocal FLIM System: Simultaneous FLIM of NAD(P)H and FAD*, Application note, available on [www.becker-hickl.com](http://www.becker-hickl.com) (2018)
36. W. Becker, C. Junghans, A. Bergmann, *Two-Photon FLIM of Mushroom Spores Reveals Ultra-Fast Decay Component*. Application note (2021), available on [www.becker-hickl.com](http://www.becker-hickl.com).
37. M. Y. Berezin, S. Achilefu, Fluorescence lifetime measurement and biological imaging. *Chem. Rev.* 110(5), 2641-2684 (2010)
38. D.K. Bird, L. Yan, K. M. Vrotsos, K. E. Eliceiri, E. M. Vaughan. Metabolic mapping of MCF10A human breast cells via multiphoton fluorescence lifetime imaging of coenzyme NADH. *Cancer Res* 65:8766–8773 (2005)
39. T. S. Blacker, Z. F. Mann, J. E. Gale, M. Ziegler, A. J. Bain, G. Szabadkai, M. R. Duchon, Separating NADH and NADPH fluorescence in live cells and tissues using FLIM. *Nature Communications* 5, 3936-1 to -6 (2014)
40. B. Chance, B. Schoener, R. Oshino, F. Itshak, Y. Nakase, Oxidation–reduction ratio studies of mitochondria in freeze-trapped samples. NADH and flavoprotein fluorescence signals *J. Biol. Chem.* 254, 4764–4771 (1979)
41. D. Chorvat, A. Chorvatova, Multi-wavelength fluorescence lifetime spectroscopy: a new approach to the study of endogenous fluorescence in living cells and tissues. *Laser Phys. Lett.* 6 175-193 (2009)
42. Y. Dancik, A. Favre, C. J. Loy, A.V. Zvyagin, M.S. Roberts, Use of multiphoton tomography and fluorescence lifetime imaging to investigate skin pigmentation in vivo. *J. Biomed. Opt.* 18(2) 026022-1 to -13 (2013)
43. M. A. Digman, V. R. Caiolfa, M. Zamai, and E. Gratton, The phasor approach to fluorescence lifetime imaging analysis, *Biophys J* 94, L14-L16 (2008)
44. R. I. Dmitriev, A. V. Zhdanov, Y. M. Nolan, D. B. Papkovsky, Imaging of neurosphere oxygenation with phosphorescent probes. *Biomaterials* 34, 9307-9317 (2013)
45. R. I. Dmitriev, A. V. Kondrashina, K. Koren, I. Klimant, A. V. Zhdanov, J. M. P. Pakan, K. W. McDermott, D. B. Papkovsky, Small molecule phosphorescent probes for O<sub>2</sub> imaging in 3D tissue models. *Biomater. Sci.* 2, 853-866 (2014)
46. R. I. Dmitriev, S. M. Borisov, A. V. Kondrashina, J. M. P. Pakan, U. Anilkumar, J. H. M. Prehn, A. V. Zhdanov, K. W. McDermott, I. Klimant, D. B. Papkovsky, Imaging oxygen in neural cell and tissue models by means of anionic cell-permeable phosphorescent nanoparticles. *Biomaterials* 34, 9307-9317 (2013)
47. R. I. Dmitriev, A. V. Kondrashina, K. Koren, I. Klimant, A. V. Zhdanov, J. M. P. Pakan, K. W. McDermott, D. B. Papkovsky, Small molecule phosphorescent probes for O<sub>2</sub> imaging in 3D tissue models. *Biomater. Sci.* 2, 853-866 (2014)
48. R. I. Dmitriev and D. B. Papkovsky, Intracellular probes for imaging oxygen concentrations: how good are they? *Methods Appl. Fluoresc.* 3, 034001-034010 (2015)
49. R. I. Dmitriev, S. M. Borisov, H. Dössmann, S. Sun, B. J. Müller, J. Prehn, V. P. Baklaushev, I. Klimant, D. B. Papkovsky, Versatile Conjugated Polymer Nanoparticles for High-Resolution O<sub>2</sub> Imaging in Cells and 3D Tissue Models. *ACS Nano* 9, 5275–5288 (2015)
50. R. I. Dmitriev and D. B. Papkovsky, Multi-parametric O<sub>2</sub> Imaging in Three-Dimensional Neural Cell Models with the Phosphorescent Probes. In: Laura Lossi and Adalberto Merighi (eds.), *Neuronal Cell Death: Methods and Protocols*, *Methods in Molecular Biology*, vol. 1254, DOI 10.1007/978-1-4939-2152-2\_5, Springer Science+Business Media New York (2015)
51. I.N. Druzhkova, M.V. Shirmanova, M.M. Lukina, V.V. Dudenkova, N. M. Mishina, E.V. Zagaynova, The metabolic interaction of cancer cells and fibroblasts – coupling between NAD(P)H and FAD, intracellular pH and hydrogen peroxide. *Cell Cycle*, 15:9, 1257-1266, (2016)
52. S. Felekyan, Software package for multiparameter fluorescence spectroscopy, full correlation and multiparameter imaging. Available from [www.mpc.uni-duesseldorf.de/seidel/software.htm](http://www.mpc.uni-duesseldorf.de/seidel/software.htm)
53. Th. Förster, Zwischenmolekulare Energiewanderung und Fluoreszenz, *Ann. Phys. (Serie 6)* 2, 55-75 (1948)
54. S. Frere, I. Slutsky, Calcium imaging using Transient Fluorescence-Lifetime Imaging by Line-Scanning TCSPC. In: W. Becker (ed.) *Advanced time-correlated single photon counting applications*. Springer, Berlin, Heidelberg, New York (2015)
55. T. Hellerer, New ultrachrome light source for microscopy, *Laser+Photonics* 4, 36-38, 2009
56. J. Jenkins, R. I. Dmitriev, D. B. Papkovsky, Imaging Cell and Tissue O<sub>2</sub> by TCSPC-PLIM. In: W. Becker (ed.) *Advanced time-correlated single photon counting applications*. Springer, Berlin, Heidelberg, New York (2015)

57. S. Kalinina, V. Shcheslavskiy, W. Becker, J. Breymayer, P. Schäfer, A. Rück, Correlative NAD(P)H-FLIM and oxygen sensing-PLIM for metabolic mapping. *J. Biophotonics* 9(8):800-811 (2016)
58. V. Katsoulidou, A. Bergmann, W. Becker, How fast can TCSPC FLIM be made? *Proc. SPIE* 6771, 67710B-1 to 67710B-7
59. K. Koenig, Clinical multiphoton tomography. *J. Biophoton.* 1, 13–23 (2008)
60. K. Koenig, A. Uchugonova, Multiphoton Fluorescence Lifetime Imaging at the Dawn of Clinical Application. In: A. Periasamy, R.M. Clegg, eds., *FLIM Microscopy in Biology and Medicine*. CRC Press 2009
61. E. I. Koshel, P. S. Chelushkin, A. S. Melnikov, P. Y. Serdobintsev, A. Yu. Stolbovaia, A. F. Saifitdinova, V. I. Shcheslavskiy, O. r Chernyavskiy, E. R. Gaginskaya, I. O. Koshevoy, S. P. Tunik, Lipophilic phosphorescent gold(I) clusters as selective probes for visualization of lipid droplets by two-photon microscopy. *Journal of Photochemistry and Photobiology A: Chemistry* 332 (2017) 122–130
62. H. Kurokawa, H. Ito, M. Inoue, K. Tabata, Y. Sato, K. Yamagata, S. Kizaka-Kondoh, T. Kadonosono, S. Yano, M. Inoue & T. Kamachi, High resolution imaging of intracellular oxygen concentration by phosphorescence lifetime, *Scientific Reports* 5, 1-13 (2015)
63. J.R. Lakowicz, H. Szmanski, K. Nowaczyk, M.L. Johnson, Fluorescence lifetime imaging of free and protein-bound NADH, *PNAS* 89, 1271-1275 (1992)
64. J.R. Lakowicz, *Principles of Fluorescence Spectroscopy*, 3rd edn., Springer (2006)
65. M. Lukina, A. Orlova, M. Shirmanova, D. Shirokov, A. Pavlikov, A. Neubauer, H. Studier, W. Becker, E. Zagaynova, T. Yoshihara, S. Tobita, V. Shcheslavskiy, Interrogation of metabolic and oxygen states of tumors with fiber-based luminescence lifetime spectroscopy. *Optics Letters* 42(4) 731-734 (2017)
66. M. M. Lukina, V. V. Dudenkova, N. I. Ignatovaa, I. N. Druzhkova, L. E. Shimolina, E. V. Zagaynovaa, M. V. Shirmanova, Metabolic cofactors NAD(P)H and FAD as potential indicators of cancer cell response to chemotherapy with paclitaxel. *BBA – General Subjects* 1862, 1693-1700 (2018)
67. D. B. Papkovsky, and R. I. Dmitriev, Biological detection by optical oxygen sensing, *Chem Soc Rev* 42, 8700-8732 (2013)
68. R.J. Paul, H. Schneckenburger, Oxygen concentration and the oxidation-reduction state of yeast: Determination of free/bound NADH and flavins by time-resolved spectroscopy, *Naturwissenschaften* 83, 32-35 (1996)
69. R. Richards-Kortum, R. Drezek, K. Sokolov, I. Pavlova, M. Follen, Survey of endogenous biological fluorophores. In M.-A. Mycek, B.W. Pogue (eds.), *Handbook of Biomedical Fluorescence*, Marcel Dekker Inc. New York, Basel, 237-264 (2003)
70. Roberts, M. S., Dancik, Y., Prow, T.W., Thorling, C.A., Li, L., Grice, J.E., Robertson, T.A., König, K., Becker, W. Non-invasive imaging of skin physiology and percutaneous penetration using fluorescence spectral and lifetime imaging with multiphoton and confocal microscopy. *European Journal of Pharmaceutics and Biopharmaceutics* 77, 469-488 (2011)
71. A. Rück, C. Hauser, S. Mosch, S. Kalinina, Spectrally resolved fluorescence lifetime imaging to investigate cell metabolism in malignant and nonmalignant oral mucosa cells. *J. Biomed. Opt.* 19(9), 096005-1 to -9 (2014)
72. W. Y. Sanchez, M. Pastore, I. Haridass, K. König, W. Becker, M. S. Roberts, Fluorescence Lifetime Imaging of the Skin. In: W. Becker (ed.) *Advanced time-correlated single photon counting applications*. Springer, Berlin, Heidelberg, New York (2015)
73. T. Sanchez, T. Wang, M. Venturas Pedro, M. Zhang, E. Esencan, D. Sakkas, D. Needleman, E. Seli, Metabolic imaging with the use of fluorescence lifetime imaging microscopy (FLIM) accurately detects mitochondrial dysfunction in mouse oocytes. *Reproductive Science* 110, 1387-1397 (2018)
74. V. I. Shcheslavskiy, A. Neubauer, R. Bukowiecki, F. Dinter, W. Becker, Combined fluorescence and phosphorescence lifetime imaging. *Appl. Phys. Lett.* 108, 091111-1 to -5 (2016)
75. V. I. Shcheslavskiy, M. V. Shirmanova, V. V. Dudenkova, K. A. Lukyanov, A. I. Gavrina, A. V. Shumilova, E. Zagaynova, W. Becker, Fluorescence time-resolved macroimaging. *Opt. Lett.* 43, No. 13, 3152-3155 (2018)
76. E. A. Shirshin, B. P. Yakimov, M. E. Darvin, N. P. Omelyanenko, S. A. Rodionov, Y. I. Gurfinkel, J. Lademann, V. V. Fadeev, and A. V. Priezhev, Label-Free Multiphoton Microscopy: The Origin of Fluorophores and Capabilities for Analyzing Biochemical Processes. *Biochemistry (Moscow)* 84, S69-S88 (2019)
77. M. C. Skala, K. M. Riching, D. K. Bird, A. Dendron-Fitzpatrick, J. Eickhoff, K. W. Eliceiri, P. J. Keely, N. Ramanujam, In vivo multiphoton fluorescence lifetime imaging of protein-bound and free nicotinamide adenine dinucleotide in normal and precancerous epithelia. *J. Biomed. Opt.* 12 02401-1 to 10 (2007)
78. M. C. Skala, K. M. Riching, A. Gendron-Fitzpatrick, J. Eickhoff, K. W. Eliceiri, J. G. White, N. Ramanujam, In vivo multiphoton microscopy of NADH and FAD redox states, fluorescence lifetimes, and cellular morphology in precancerous epithelia, *PNAS* 104, 19494-19499 (2007)
79. H. Studier, W. Becker, Megapixel FLIM. *Proc. SPIE* 8948 (2014)
80. C. Toncelli, O. V. Arzhakova, A. Dolgova, A. L. Volynskii, N. F. Bakeev, J. P. Kerry, D. B. Papkovsky, Oxygen-sensitive phosphorescent nanomaterials produced from high density polyethylene films by local solvent-crazing. *Anal. Chem.* 86(3), 1917-23 (2014)



## DCS-120 FLIM System

81. A. J. Walsh, A. T. Shah, J. T. Sharick, M. C. Skala, Fluorescence Lifetime measurements of NADH in live cells and tissue. In: W. Becker (ed.) Advanced time-correlated single photon counting applications. Springer, Berlin, Heidelberg, New York (2015)
82. S. Weidkamp-Peters, S. Felekyan, A. Bleckmann, R. Simon, W. Becker, R. Kühnemuth, C.A.M. Seidel. Multiparameter fluorescence image spectroscopy to study molecular interactions. Photochem. Photobiol. Sci. 8, 470-480 (2009)
83. M. Yaseen, J. Sutin, W. Wu, B. Fu, H. Uhlirova, A. Devor, D.A. Boas, S. Sakadzic, Fluorescence lifetime microscopy of NADH distinguishes alterations in cerebral metabolism in vivo. Biome. Opt. Expr. 8, 2368-2385 (2017)
84. G. Yazgan, R. I. Dmitriev, V Tyagi, J.Jenkins, G-M. Rotaru, M.Rottmar, R. . Rossi, C. Toncelli, D. B. Papkovsky, K. Maniura-Weber, G. Fortunato, Steering surface topographies of electrospun fibers: understanding the mechanisms. Scietific Reports 7, 158-1 to -13 (2017)
85. A. V. Zhdanov, A. V. Golubeva, I. A. Okkelman, J. F. Cryan, D. B. Papkovsky, Imaging of oxygen gradients in giant umbrella cells: an ex vivo PLIM study. Am J Physiol Cell Physiol 309, 2015
86. A. V. Zhdanov, I. A. Okkelman, A. V. Golubeva, B. Doerr, N. P. Hyland, S. Melgar, F. Shanahan, J. F. Cryan, D. B. Papkovsky, Quantitative analysis of mucosal oxygenation using ex vivo imaging of healthy and inflamed mammalian colon tissue. Cell. Mol. Life Sci. 74, 141–151 (2017)



### Becker & Hickl GmbH

Nunsdorfer Ring 7-9

12277 Berlin, Germany

Tel. +49 30 212 800 20, Fax. +49 30 212 800 213

email: [info@becker-hickl.com](mailto:info@becker-hickl.com), [www.becker-hickl.com](http://www.becker-hickl.com)